Available online at www.sciencedirect.com

ScienceDirect

Geochimica et Cosmochimica Acta 302 (2021) 61–82

Geochimica et Cosmochimica Acta

www.elsevier.com/locate/gca

Chalcophile element partitioning between Cu-rich sulfide phases and silicate melt and implications for the formation of Earth's continental crust

Yuan Li [a,b,*], Andreas Audétat [c], Zhiwei Liu [a,b], Fangyue Wang [d]

[a] State Key Laboratory of Isotope Geochemistry, Guangzhou Institute of Geochemistry, Chinese Academy of Sciences, Guangzhou 510640, China

[b] CAS Center for Excellence in Deep Earth Science, Guangzhou 510640, China

[c] Bayerisches Geoinstitut, Universität Bayreuth, 95440 Bayreuth, Germany

[d] School of Resources and Environmental Engineering, Hefei University of Technology, Hefei 230009, China

Received 12 July 2020; accepted in revised form 17 March 2021; available online 29 March 2021

Abstract

To constrain the behavior of chalcophile (sulfide-loving) elements during arc magmatic differentiation and to understand the formation conditions of Earth's continental crust, the partition coefficients (D) of Mn, Co, Cu, Zn, As, Se, Mo, Ag, Cd, Sn, Sb, Te, Re, Au, Pb, and Bi between monosulfide-solid-solution (MSS), Cu-rich sulfide liquid (SL; containing 11–45 wt.% Cu), and hydrous silicate melt (SM) of basaltic to dacitic compositions were determined at 1000–1200 °C, 0.5–1.0 GPa, and fO_2 1–1.5 log units above the fayalite–magnetite–quartz (FMQ) buffer. The $D^{SL/SM}$ values are 16–160 for Co, 1100–8400 for Cu, 50–220 for Se, 1200–5900 for Ag, 50–1800 for Cd, 700–3300 for Te, 15–510 for Re, 5700–90,000 for Au, 20–440 for Pb, and 140–3300 for Bi. The $D^{SL/SM}$ values for Mn, Zn, As, Mo, Sn, and Sb are below 1–40. The $D^{MSS/SM}$ values are 55–260 for Co, 530–1700 for Cu, 74–110 for Se, 30–110 for Ag, 4–40 for Cd, 15–70 for Te, 200–5900 for Re, and 140–270 for Au. The $D^{MSS/SM}$ values for Mn, Zn, As, Mo, Sn, Sb, Pb, and Bi are below 1–3. The $D^{SL/SM}$ of Au increase with increasing Cu content of the sulfide liquid, but the $D^{SL/SM}$ of the other elements little affected by the Cu concentration in the sulfide liquid. Because of their distinct dissolution mechanisms in the silicate melt, the $D^{SL/SM}$ and $D^{MSS/SM}$ of Mn, Co, Zn, Cd, Sn, and Pb are mainly controlled by the silicate melt FeO_{tot} content ([FeO_{tot}]); the $D^{SL/SM}$ and $D^{MSS/SM}$ for Re, Mo, As, Sb, and Bi are mainly controlled by [FeO_{tot}] and fO_2; the $D^{SL/SM}$ and $D^{MSS/SM}$ for Cu, Ag, and Au are mainly controlled by [FeO_{tot}] and the content of reduced sulfur in the silicate melt; and the $D^{SL/SM}$ and $D^{MSS/SM}$ for Se and Te are mainly controlled by fO_2. Using all available $D^{SL/SM}$ and $D^{MSS/SM}$ data, a partitioning model was developed for predicting $D^{SL/SM}$ and $D^{MSS/SM}$ of chalcophile elements as a multi-function of temperature, pressure, fO_2, and silicate melt and sulfide compositions. Sulfide phase relations suggest that the sulfides precipitating from arc magmas containing >100 μg/g Cu in the silicate melt occur as Cu-rich sulfide liquid, whereas the sulfides precipitating from arc magmas containing 30–70 μg/g Cu in the silicate melt occur as mixed MSS and Cu-rich sulfide liquid. Modeling the Cu evolution trends of global arc magmas illustrates that the precipitating sulfides are dominantly MSS in continental arcs with a crustal thickness of >30 km, with the proportion of sulfide liquid being less than 20%; whereas, in island arcs with a crustal thickness of <20 km, the proportion of sulfide liquid may reach up to 90%. Applying the model to predict the evolution trends of Ag, As, Sn, Sb, Se, Mo, Re, Mo, Au, Pb, and Bi in global arc magmas under various fO_2 conditions, we find that when no more than 10% of the precipitating sulfides are sulfide liquid, the chalcophile

* Corresponding author at: State Key Laboratory of Isotope Geochemistry, Guangzhou Institute of Geochemistry, Chinese Academy of Sciences, Guangzhou 510640, China.

E-mail address: Yuan.Li@gig.ac.cn (Y. Li).

https://doi.org/10.1016/j.gca.2021.03.020

element patterns of oxidized magmas (0–1 log unit above FMQ) in continental arcs match that of Earth's bulk continental crust, which implies that Earth's continental crust formed mainly in oxidized continental arcs.

Keywords: Chalcophile elements; Sulfides; Partition coefficients; Arc magmas; Subduction zones

1. INTRODUCTION

Earth is unique among the rocky planets in the inner solar system in that it has an andesitic continental crust (Taylor and McLennan, 2009). Comparisons of the geochemical data of Earth's continental crust with the present-day composition of lavas in different tectonic settings indicate that Earth's continental crust formed in subduction-related volcanic arcs, or via a geochemical process very similar to the arc magmatic process today (Rudnick, 1995; Hawkesworth et al., 2010; Rudnick and Gao, 2014; Jagoutz and Kelemen, 2015). However, the net flux from Earth's mantle into arc crust is basaltic rather than andesitic. Therefore, additional mechanisms are required to transform Earth's mantle-derived basaltic melt into andesitic continental crust. Relamination of buoyant subducting felsic materials (Kelemen and Behn, 2016), and delamination of dense cumulates from the base of arc crust (Jagoutz and Behn, 2013; Lee, 2014), are proposed to be the two main mechanisms to account for this transformation. Nevertheless, the physical and chemical conditions for relamination or delamination remain unclear. Consequently, the conditions for the formation of Earth's continental crust remain an unresolved issue.

Chalcophile element systematics of arc magmas are powerful tools to constrain a range of processes and parameters, including the differentiation of Earth's mantle and crust (Li and Audétat, 2012, 2015; Jenner, 2017; Wang et al., 2018), and the oxidization state of the mantle and mantle-derived magmas (Lee et al., 2012; Feng and Li, 2019). However, these constraints rely on knowledge of the chemical behavior of chalcophile elements in arc magmas under various pressure (P), temperature (T), and oxygen fugacity (fO_2) conditions, which is largely controlled by sulfides. Therefore, to better understand the chemical behavior of chalcophile elements in arc magmas, and the formation conditions of Earth's continental crust as an application, partition coefficients of chalcophile elements between sulfides and silicate melt need to be known for various P–T–fO_2–composition conditions. Previous studies have shown that sulfides are ubiquitous in variably evolved arc magmatic rocks (Wallace and Edmonds, 2011; Parat et al., 2011; Lee et al., 2012; Chang and Audétat, 2018; Williams et al., 2018). For example, during arc magmatic differentiation, the decrease of the Cu content with decreasing MgO (wt.%) is caused by segregation of sulfides (Lee et al., 2012; Li and Audétat, 2013; Chiaradia, 2014). Depending on pressure, temperature, and sulfide composition (Cu and/or Ni contents), magmatic sulfides can occur as monosulfide solid solution (MSS) and/or sulfide liquid (Kullerud et al., 1969; Kullerud, 1970; Bockrath et al., 2004; Li and Audétat, 2012, 2015; Zhang and Hirschmann, 2016). MSS was proposed to be qualitatively more abundant than sulfide liquid during arc magmatic differentiation (Li and Audétat, 2013; Wang et al., 2018). However, the presence of up to 250 μg/g Cu in differentiated arc magmas (Lee et al., 2012; Chiaradia, 2014; Li, 2014a; Agangi and Reddy, 2016) and consequently, the presence of a few to a few tens wt.% of Cu in the coexisting sulfides can potentially stabilize Cu-rich sulfide liquid. The coexistence of MSS and Cu-rich sulfide liquid has indeed been observed in many oxidized arc magmas (Hattori, 1993; Audetat and Pettke, 2006; Agangi and Reddy, 2016; Chang and Audétat, 2018; Georgatou et al., 2018). Therefore, in order to quantitatively understand the behavior of chalcophile elements in arc magmas, partition coefficients of chalcophile elements between sulfide phases including both MSS and sulfide liquid and silicate melt of various compositions should be determined under various P–T–fO_2 conditions.

Early studies measuring the partition coefficients of Cu, Ni, Co, Pb, Mo, and Zn between sulfide liquid and simplified silicate melt ($D^{SL/SM}$) were performed under dry and/or ambient pressure conditions (Rajamani and Naldrett, 1978; Gaetani and Grove, 1997; Ripley et al., 2002). A few later studies determined the partitioning of Cu, Au, Ag, W, and Mo between pyrrhotite and basaltic to rhyolitic melt (Simon et al., 2008; Bell et al., 2009; Mengason et al., 2011; Botcharnikov et al., 2011; Zajacz et al., 2013; Botcharnikov et al., 2013). More recently, Kiseeva and Wood (2013, 2015) investigated the effects of temperature and silicate melt FeO content on $D^{SL/SM}$ for Cu, In, Tl, Pb, Ag, Mn, Zn, Cr, Co, Ni, Sb, and Cd at 1300–1700 °C and 1.5 GPa. Li and Audétat (2012, 2013, 2015), Botcharnikov et al. (2013), and Feng and Li (2019) reported $D^{SL/SM}$ and $D^{MSS/SM}$ for V, Mn, Co, Ni, Cu, Zn, As, Mo, Ag, Sn, Sb, W, Re, Au, Pb, and Bi in the hydrous basanitic/basaltic to rhyolitic melt systems at 900–1300 °C and 0.5–3 GPa. Brenan (2015) measured $D^{SL/SM}$ and $D^{MSS/SM}$ for Se and Te at 1200–1300 °C and 0.9–1.5 GPa. Li et al. (2019) measured $D^{MSS/SM}$ for Au at 950–1050 °C and 0.5–3 GPa at various fO_2. However, previous experiments do not contain sulfide liquid at temperatures below 1100 °C, and none of the previous studies has focused on measuring the partition coefficients of chalcophile elements between Cu-rich sulfide phases and silicate melt under conditions appropriate for oxidized arc magmatism.

Here we perform experiments to measure the partition coefficients of Mn, Co, Cu, Zn, As, Se, Mo, Ag, Cd, Sn, Sb, Re, Au, Te, Pb, and Bi between Cu-rich sulfide phases and hydrous basaltic to dacitic melts under conditions appropriate for oxidized arc magmatism. In conjunction with literature data, the new partitioning data are used to

place constraints on the fate of chalcophile elements during arc magmatic differentiation and the formation conditions of Earth's continental crust.

2. EXPERIMENTAL METHODS

2.1. Starting materials

Starting materials include natural rocks and synthetic silicate glasses, synthetic Cu–Fe–S sulfides, distilled water, and reagent-grade $CaSO_4$ (anhydrite). The synthetic silicate glasses have major element composition similar to that of average mid-ocean ridge basalt (MORB) and arc dacite and were prepared from analytical-grade oxides (MgO, FeO, MnO, NiO, SiO_2, TiO_2, Al_2O_3, Cr_2O_3, and P_2O_5) and carbonates (Na_2CO_3, K_2CO_3, and $CaCO_3$). The natural rock was a partly glassy andesite. The starting Cu–Fe–S sulfides with 10–45 wt.% Cu were synthesized from mixtures of FeS, CuS, and Fe powder at 1250 °C and 1.0 GPa for 20 minutes in a graphite-lined $Pt_{95}Rh_{05}$ capsule. Before synthesis, trace amounts of Co, Zn, As, Se, Mo, Ag, Cd, Sn, Sb, Te, Re, Au, Te, Pb, and Bi were doped in the FeS–CuS–Fe mixtures by adding metallic powder or metal sulfides. Major and trace element compositions of the starting silicates and sulfides are given in Table 1. All silicates and sulfides were ground into powder and mixed before loading into sample capsules.

2.2. Sample capsule and P-T conditions

Starting mixtures of ~67–70 wt.% silicate, ~20 wt.% sulfide, and ~5 wt.% anhydrite were loaded into olivine capsules, which were then placed into $Pt_{95}Rh_{05}$ capsules that were eventually sealed by arc welding. Approximately 5 wt.% distilled water relative to the mass of the silicate was also added into the olivine capsules using a syringe to generate hydrous silicate melt. The use of olivine capsules was to effectively minimize the reaction between samples and the $Pt_{95}Rh_{05}$ sample capsules (Li and Audétat, 2012, 2013). The addition of ~5 wt.% anhydrite was to obtain sample fO_2 associated with oxidized arc magmatism (Parat et al., 2011; Chang and Audétat, 2018). The experiments were performed at 1100–1200 °C and 1 GPa for the sulfide–basalt system, and at 1000–1100 °C and 0.5 GPa for the sulfide–dacite/andesite system. Detailed P–T conditions and starting mixture for each individual experiment are summarized in Table 2.

The experimental durations were 20–24 hours for experiments at 1200 °C, 24–45 hours for experiments at 1100 °C, and 42–90 hours for experiments at 1000 °C. These experimental durations have been shown to be sufficiently long for reaching equilibrium partitioning of chalcophile elements between sulfide phases and silicate melt (Mengason et al., 2011; Li and Audétat, 2012; Kiseeva and Wood, 2013; Zajacz et al., 2013; Li and Audétat, 2015). The homogeneous distribution of major and trace elements in the sulfide phases and silicate melt, and the consistence in the partition coefficients obtained in this study and previous studies, as will be shown below, also demonstrate the attainment of equilibrium partitioning in this study.

2.3. High-pressure equipment

All experiments were conducted in an end-loaded, solid-media piston cylinder apparatus (Max Voggenreiter LPC250), using 0.5-in. diameter MgO–NaCl assemblies with stepped graphite heaters as described in previous studies (Li and Audétat, 2012, 2013, 2015). A friction correction of 5% was applied to the nominal pressure based on a calibration of the quartz–coesite transition (Li and Audétat, 2012), and the hot piston-in method was used to pressurize the assembly. The total pressure uncertainty was less than 0.1 GPa. Experimental temperatures were monitored by S-type thermocouples with an uncertainty of ~10 °C. All experiments were quenched to below 100 °C within 10–20 seconds by switching off the electric power to the graphite heaters.

Table 1
Major and trace element compositions of the starting silicates and sulfides.

Silicates				Sulfides			
	MORB	Andesite	Dacite		Sulf (Cu10)	Sulf (Cu30)	Sulf (Cu45)
SiO_2	50.07	59.1	65.74	Cu	10.0	30.0	45.0
TiO_2	1.66	0.94	0.5	Fe	55.0	40.0	25.0
Al_2O_3	15.38	17.8	16.68	S	35.0	30.0	30.0
FeO	10.8	6.43	5.33	Total	100.0	100.0	100.0
MnO	0.02	0.1	0.02	Trace elements doped in sulfides			
MgO	6.8	3.05	2.13	Ni	2000	Cd	400
CaO	11.61	6.85	4.09	Co	1000	Sb	300
Na_2O	2.83	4.27	3.31	Zn	200	Sn	300
K_2O	0.23	1.08	1.69	As	500	Pb	300
P_2O_5	0.3	0.22	0.06	Se	1000	Bi	1000
NiO	0.03	n.a	0.04	Te	1000	Re	700
Cr_2O_3	0.01	n.a	0.06	Ag	1000	Mo	300
Total	99.74	100.12	99.69	Au	2000		

Oxides in silicates and Fe, S, and Cu in sulfides are in wt.%; trace elements in sulfides are in μg/g.

Table 2
Summary of experimental conditions and products.

Exp. No	Temperature °C	Pressure GPa	[a]Starting composition	[b]Sample capsule	Run duration Hours	[c]Run products	[d]Sample fO_2 ΔFMQ	[e]NBO/T	[#]S in silicate melt μg/g	[#]S^{6+}/S_{tot}
Cu02-1	1200	1.0	MORB + ~5%Anhy + 30%Sulf(Cu10) + ~5%H_2O	$Pt_{95}Rh_{05}$ + Olivine	23	Glass + MSS + SL + Anhy + Crystal	>1–1.5	0.57	5566 ± 246	0.77 ± 0.09
Cu02-2	1200	1.0	MORB + ~5%Anhy + 30%Sulf(Cu45) + ~5%H_2O	$Pt_{95}Rh_{05}$ + Olivine	23	Glass + SL + Crystal	>1–1.5	0.69	4139 ± 140	0.68 ± 0.07
Cu05	1200	1.0	MORB + ~5%Anhy + 30%Sulf(Cu45) + ~5%H_2O	$Pt_{95}Rh_{05}$ + Olivine	20	Glass + SL + Anhy + Crystal	>1–1.5	0.82	6232 ± 368	0.73 ± 0.07
Cu06	1100	1.0	MORB + ~5%Anhy + 30%Sulf(Cu10) + ~5%H_2O	$Pt_{95}Rh_{05}$ + Olivine	24	Glass + MSS + SL + Anhy + Crystal	>1–1.5	0.64	9747 ± 117	0.69 ± 0.08
Cu07	1100	1.0	MORB + ~5%Anhy + 30%Sulf(Cu45) + ~5%H_2O	$Pt_{95}Rh_{05}$ + Olivine	24	Glass + SL + Anhy + Crystal	>1–1.5	0.82	6232 ± 368	0.76 ± 0.06
Cu08	1000	0.5	Dacite + ~5%Anhy + 30%Sulf(Cu10) + ~5%H_2O	$Pt_{95}Rh_{05}$ + Olivine	45	Glass + MSS + SL + Fluid + Crystal	>1–1.5	0.11	260 ± 20	n.d.
Cu09	1000	0.5	Dacite + ~5%Anhy + 30%Sulf(Cu45) + ~5%H_2O	$Pt_{95}Rh_{05}$ + Olivine	45	Glass + SL + Crystal	>1–1.5	0.12	519 ± 105	0.62 ± 0.15
Cu10	1100	0.5	Dacite + ~5%Anhy + 30%Sulf(Cu10) + ~5%H_2O	$Pt_{95}Rh_{05}$ + Olivine	45	Glass + MSS + SL + Fluid + Crystal	>1–1.5	0.29	949 ± 91	0.63 ± 0.06
Cu11	1000	0.5	Andesite + ~5%Anhy + 30%Sulf(Cu10) + ~5%H_2O	$Pt_{95}Rh_{05}$ + Olivine	45	Glass + MSS + SL + Anhy + Crystal	>1–1.5	0.09	730 ± 89	n.d.
Cu12	1100	0.5	Dacite + ~5%Anhy + 30%Sulf(Cu45) + ~5%H_2O	$Pt_{95}Rh_{05}$ + Olivine	24	Glass + SL + Anhy + Crystal	>1–1.5	0.31	1003 ± 218	0.57 ± 0.15
Cu13	1200	1.0	MORB + ~5%Anhy + 30%Sulf(Cu30) + ~5%H_2O	$Pt_{95}Rh_{05}$ + Olivine	24	Glass + SL + Anhy + Crystal	>1–1.5	0.93	8801 ± 171	0.86 ± 0.09
Cu14	1100	1.0	MORB + ~5%Anhy + 30%Sulf(Cu30) + ~5%H_2O	$Pt_{95}Rh_{05}$ + Olivine	25	Glass + SL + Anhy + Crystal	>1–1.5	0.73	12,944 ± 810	0.91 ± 0.07
Cu15	1000	0.5	Dacite + ~5%Anhy + 30%Sulf(Cu30) + ~5%H_2O	$Pt_{95}Rh_{05}$ + Olivine	90	Glass + SL + Anhy + Crystal	>1–1.5	0.12	720 ± 100	n.d.
Cu16	1100	0.5	Dacite + ~5%Anhy + 30%Sulf(Cu30) + ~5%H_2O	$Pt_{95}Rh_{05}$ + Olivine	42	Glass + SL + Fluid + Crystal	>1–1.5	0.32	1430 ± 212	0.55 ± 0.16

a:Anhy = anhydrite; Sulf(Cu10) = Fe-Cu-S sulfide with 10 wt.% Cu. b: an inner olivine capsule plus an outer Pt95Rh05 capsule.
c: Glass = silicate glass; MSS = crystalline monosulfide solid solution; SL = Cu-rich sulfide liquid; Crystal = silicate crystals of clinopyroxene ± olivine ± amphibole; Fluids means that the sample was saturated with a fluid phase.
d: see text for the estimation of sample fO_2. e: Silicate melt NBO/T = 2Total O/T − 4 (T = Si + Ti + Al + Cr + P).
n.d: not determined because of the low S content in the silicate melt. The errors for S in silicate melt and S^{6+}/S_{tot} are 1σ standard deviation based on the replicate analyses.
1σ standard deviation was based on the replicate analyses.

2.4. Analytical methods

2.4.1. Electron microprobe

Major element compositions of the quenched sulfide phases and silicate melts were measured with a JEOL JXA-8200 microprobe, using wavelength-dispersive mode and a PAP matrix correction. Sulfides were analyzed with 20 kV acceleration voltage and 20nA beam current, whereas quenched silicate melts were analyzed with 15 kV/10nA. Natural and synthetic standards were used to calibrate the instrument. For sulfide analysis, Fe and S were calibrated on a synthetic pyrrhotite with well-known Fe: S ratio, Ni, Co, and Cu were calibrated on pure metals, and O was calibrated on magnetite. For silicate melts, Na was calibrated on albite, Ca on wollastonite, K on orthoclase, Ti and Mn on ilmenite, Si on enstatite, Mg on forsterite, Al on spinel, P on GaP, and Fe on metallic Fe. Sulfur in quenched silicate melts was analyzed with 50 nA beam current and 60 s peak counting time using barite as standard. A defocused beam of 30 μm diameter was used for all the standardizations and sample measurements.

The oxidation state of S in the silicate melt was determined with 30 nA beam current and a defocused beam of 20 μm based on the shift of the SK_α lines with respect to the $BaSO_4$ (S^{6+}) and the ZnS (S^{2-}) standards (Carroll and Rutherford, 1988). The ratio S^{6+}/S_{total} is given by:

$$\frac{S^{6+}}{S_{total}} = \frac{\Delta\lambda(SK_\alpha)_{glass}}{\Delta\lambda(SK_\alpha)_{sulfate}} \times 100\% \quad (1)$$

where $\Delta\lambda(SK_\alpha)_{glass}$ is the wavelength shift of the measured glass sample relative to ZnS and $\Delta\lambda(SK_\alpha)_{sulfate}$ is the wavelength shift of $BaSO_4$ relative to the same reference. Measurements of the SK_α position were carried out on a PETJ spectrometer, which was moved over a range of ~3.12 * 10^{-2} Å in 100–200 steps, using 500 ms counting time for each step (total acquisition time was between 50 s and 100 s).

2.4.2. LA–ICP–MS

Major and trace elements of the quenched sulfide phases and silicate melts were analyzed by laser–ablation ICP–MS, using a GeolasPro 193 nm ArF Excimer laser (Coherent/Lambda Physik) attached to an Elan DRC-e quadrupole mass spectrometer (Perkin Elmer Instruments). The laser with beam sizes of 20–50 μm was operated at a frequency of 10 Hz and an energy of 80 mJ for quenched silicate melts, and at 7 Hz and 70 mJ for sulfides. The sample chamber was flushed with He at a rate of 0.4 L/min, to which 5 ml/min H_2 was added on the way to the ICP-MS. Dwell times were 10 ms for the isotopes ^{23}Na, ^{24}Mg, ^{27}Al, ^{29}Si, ^{39}K, ^{42}Ca, ^{49}Ti, ^{55}Mn, ^{57}Fe, ^{59}Co, ^{62}Ni, ^{65}Cu, ^{66}Zn, ^{75}As, ^{82}Se, ^{98}Mo, ^{107}Ag, ^{111}Cd, ^{118}Sn, ^{121}Sb, ^{125}Te, ^{208}Pb and ^{209}Bi, and 20 ms for ^{197}Au. At these analytical conditions, Se, Te, and Au in silicate melts of most of our experiments were below the detection limit. We later carried out further analyses of ^{23}Na, ^{24}Mg, ^{27}Al, ^{29}Si, ^{39}K, ^{42}Ca, ^{49}Ti, ^{55}Mn, ^{57}Fe, ^{59}Co ^{65}Cu, ^{75}As, ^{82}Se, ^{111}Cd, ^{125}Te, and ^{197}Au in silicate melts using an Agilent 7900 Quadrupole ICP-MS coupled to a Photon Machines Analyte HE 193-nm ArF Excimer Laser Ablation system (Li, 2018). Helium was applied as the carrier gas (0.9 L/min) and mixed with the Ar carrier gas (0.85 L/min) via a T-connector before entering the ICP. After measuring the gas blank for 20 s, each analysis was performed by a laser beam of 60–100 μm diameter, at 8 Hz with an energy of ~2 J/cm^2 for 40 s for silicate melts. The dell times for ^{82}Se, ^{125}Te, and ^{197}Au were increased to 30 ms, so that we were able to push the detection limit down to 2.5 μg/g for ^{82}Se, 0.1 μg/g for ^{125}Te, and 0.01 μg/g for ^{197}Au, respectively. The respective contributions of ^{91}Zr^{16}O and ^{40}Ca^{42}Ca to our measured ^{107}Ag and ^{82}Se are negligible because of the relatively high Ag and Se concentrations in our samples. NIST SRM 610 glass was used as external standard for all analyses, whereas Si and Fe determined by electron microprobe were used as internal standard for silicate melts and sulfides, respectively. Overall uncertainties arising from the internal and external standardization procedures are estimated at 15–20% for all elements 2–3 times above the detection limit (Li and Audétat, 2012). Elements that were analyzed in both LA–ICP–MS facilities agreed within 5% relative.

3. RESULTS

3.1. Sample petrography

Experimental conditions and products are summarized in Table 2, and representative textures are shown in Fig. 1. Sulfide and silicate melt coexisted in all experiments. A few % to up to ~50% of olivine and clinopyroxene crystals were produced in the experiments starting with basalt at 1100–1200 °C, and a few % of clinopyroxene ± olivine ± amphibole crystals were produced in the experiments starting with dacite and andesite. A fluid phase occurred in the experiments at 0.5 GPa (runs Cu08, Cu10, Cu12, and Cu16), as evidenced by the presence of vesicles in the quenched silicate melt. Anhydrite crystals were not found in the experiments saturated with a fluid phase, which could be due to the strong partitioning of S into the fluid phase (Zajacz et al., 2013; Masotta et al., 2016).

Two different sulfide phases were produced (Fig. 1). One was crystalline Fe–Cu–S sulfide and the other was Cu-rich Fe–Cu–S sulfide liquid, both with size up to 1000 μm. The crystalline Fe–Cu–S sulfide will be referred to as MSS hereafter because the Cu content in the crystalline sulfide is ≤5 wt.% (see below). MSS is a homogeneous solid with smooth surface (Fig. 1b and c). During experimental quench, sulfide liquid always unmixed into fine-grained phases of Cu-poor MSS (5–30 μm) and chalcopyrite/chalcocite when the sulfide liquid contained ≤30 wt.% Cu (Fig. 1c), and into intermediate solid solution and Cu_2S when the sulfide liquid contained ~45 wt.% Cu (Fig. 1d). As shown in Fig. 1c, the MSS grains exsolved from sulfide liquid during quench are irregular in shape and embedded in chalcopyrite/chalcocite, and they are in texture clearly distinct from the crystalline MSS. Crystalline MSS and Cu-rich sulfide liquid coexisted in the experiments starting with sulfide containing 10 wt.% Cu, whereas only Cu-rich sulfide liquid existed in the experiments starting with sulfide containing 30 or 45 wt.% Cu (Table 2).

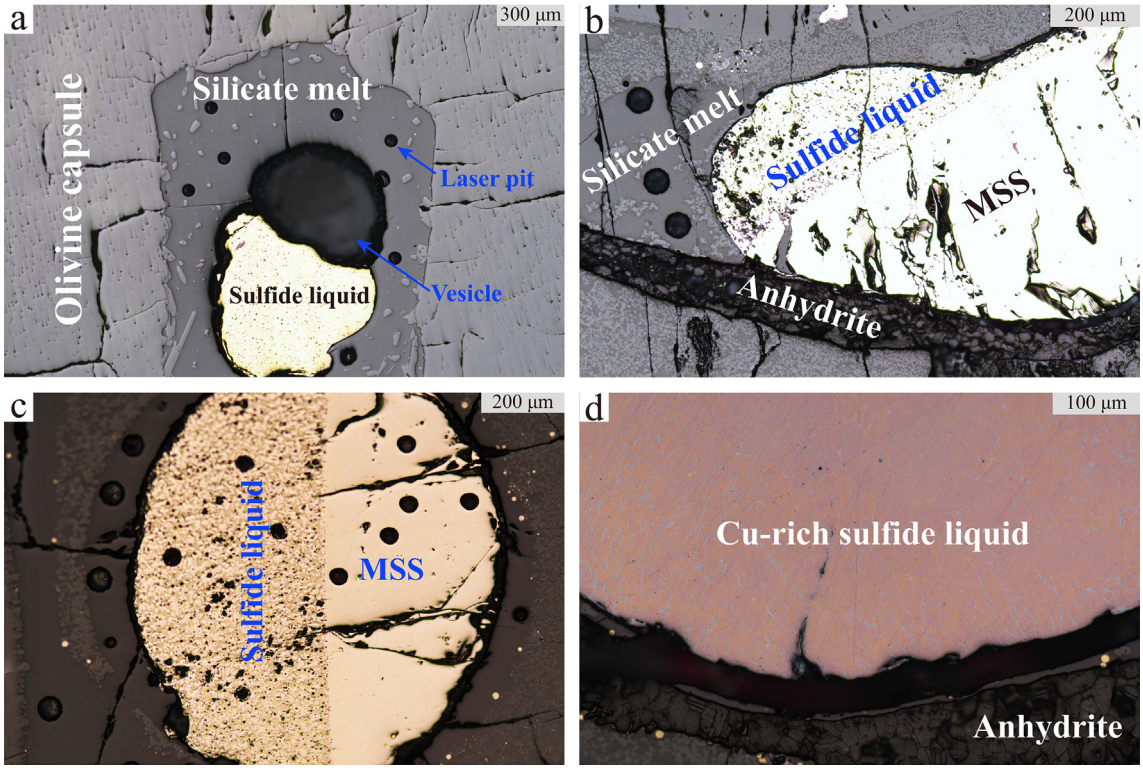

Fig. 1. Reflected-light photomicrographs of typical run products in olivine-lined $Pt_{95}Rh_{05}$ capsules. (a) The coexistence of dacitic melt, silicate crystals, sulfide liquid with ~31.5 wt.% Cu, and a large vesicle (Run Cu16 at 1100 °C and 0.5 GPa). The large vesicle indicates saturation in a fluid phase during the run. (b) The coexistence of basaltic melt, silicate crystals, crystalline MSS with 3.9 wt.% Cu, sulfide liquid with 12.3 wt.% Cu, and anhydrite crystals (Run Cu06 at 1100 °C and 1 GPa). (c) The coexistence of crystalline MSS with 4.0 wt.% Cu and sulfide liquid with 11.2 wt.% Cu (Run Cu02-1 at 1200 °C and 1 GPa). Note that crystalline MSS is quenched into homogeneous solid with size up to a few hundreds of μm, whereas sulfide liquid always exsolves minor phases. The MSS grains (5–30 μm) exsolved from sulfide liquid during quench are irregular in shape and are clearly different from the crystalline MSS in texture. (d) The texture of sulfide liquid with 44.6 wt.% Cu (Run Cu07 at 1100 °C and 1 GPa). The high-Cu sulfide liquid unmixed into intermediate solid solution and Cu_2S during quench. Also note that the sulfide liquid with 44.6 wt.% Cu is purplish, but the sulfide liquid with 11.2–31.5 wt.% Cu is yellowish.

3.2. Major and trace element compositions of silicate melts

Major and trace element compositions of the quenched silicate melts are summarized in Tables S1 and S2. Major elements of the silicate melts were similar those of the starting silicates. Most major elements changed less than 20% relative, except for FeO and MgO in the dacitic and andesitic melts, where they decreased up to 50% in the runs Cu08, Cu09, and Cu11 due to olivine crystallization. Silicate melt NBO/T calculated based on a hydrous basis ranged from 0.57 to 0.93 for the experiments starting with basalt, whereas it was between 0.09 and 0.32 for the experiments starting with dacite and andesite.

Based on the deficit of the EMPA totals (90.4–97.6 wt.%) from 100 wt.% (Table S1), the silicate melts contained ~3–10 wt.% H_2O. The S content ranged from 4100 to 12,900 μg/g in basaltic melts, and from 260 to 1430 μg/g in andesitic to dacitic melts (Table 2). The S content in the silicate melts increases with increasing NBO/T, as has been observed for anhydrite solubility in silicate melts (Masotta and Keppler, 2015). The S^{6+}/S_{tot} ranged from 0.68 to 0.91 in basaltic melts, and from 0.55 to 0.63 in andesitic to dacitic melts (Table 2). The S^{6+}/S_{tot} in silicate melts of runs Cu08, Cu11, and Cu15 could not be determined because of the relatively low S content. The measured S^{6+}/S_{tot} values are consistent with previous results obtained from basaltic to dacitic melts that were saturated with both sulfide and anhydrite (Feng and Li, 2019; Li et al., 2019).

Most trace elements were homogeneously distributed in the silicate melts. As found in previous studies (Li and Audétat, 2012; Feng and Li, 2019), the reaction between olivine capsule walls and silicate melts was negligible with respect to major and trace elements, which is probably due to the low experimental temperatures and/or the crystallization of olivine from the silicate melts. The silicate melts that were saturated with both MSS and sulfide liquid contained 28–66 μg/g Cu. In the experiments that were saturated with sulfide liquid only, the basaltic melts contained 168–338 μg/g Cu, and the andesitic to dacitic melts contained 57–316 μg/g Cu.

3.3. Major and trace element compositions of sulfides

Major and trace element compositions of the quenched sulfides are given in Table S3. Crystalline MSS, which was present in runs Cu02-1, Cu06, Cu08, Cu10, and Cu11, contained 3.9–5 wt.% Cu, 0.22–0.34 wt.% Ni, and 37.4–39.2 wt.% S. The corresponding sulfide liquid con-

tained 10.6–23.2 wt.% Cu, 0.17–0.37 wt.% Ni, and 31.8–34.5 wt.% S. In experiments where only sulfide liquid was present, the sulfide liquid contained 31.3–44.6 wt.% Cu, 0.22–0.41 wt.% Ni, and 29.2–32.8 wt.% S. Compared to MSS, sulfide liquid contained more Cu but less Fe and S.

Most of the trace elements were homogeneously distributed in sulfides at the scale of our laser beam sizes applied (20–50 μm). Sn in MSS was below the detection limit of our LA-ICP-MS (Table S4). The relatively large 1–σ error for Bi in the sulfide liquid of runs Cu08, Cu15, and Cu16, and for Pb in the sulfide liquid of run Cu08 should be caused by the heterogeneous texture of sulfide liquid produced during quench. In each experiment, Co, Mo, and Re occurred at higher concentrations in MSS than in sulfide liquid, whereas all other trace elements such as Au, Ag, Bi, Te, and Pb were more concentrated in the sulfide liquid. These observations are consistent with previous results on Cu-poor sulfide systems (Brenan, 2002; Li and Audétat, 2012; Brenan, 2015; Li and Audétat, 2015; Liu and Brenan, 2015).

3.4. Estimation of sample fO_2

Sulfide and anhydrite coexist in basaltic melt in a rather narrow range of fO_2 (~FMQ + 1.5 to FMQ + 2), and the fO_2 for stabilizing anhydrite in basaltic melt is usually larger than FMQ + 1.5 (Jugo, 2004; Jugo et al., 2010; Botcharnikov et al., 2011). Therefore, the fO_2 of our sulfide- and anhydrite-saturated experiments should be above FMQ + 1.5. The S^{6+}/S_{tot} in basaltic to dacitic melts, determined using Δλ(SKα) of electron microprobe, is mainly a function of fO_2 (Jugo et al., 2005; Wilke et al., 2011). Several studies have calibrated S^{6+}/S_{tot} in the quenched silicate melts as a function of fO_2 varying from FMQ-2 to FMQ + 6 (Carroll and Rutherford, 1988; Wallace and Carmichael, 1994; Jugo et al., 2005; Wilke et al., 2011), and these calibrations have been used to estimate the fO_2 of natural and experimentally synthesized samples of different compositions by determining S^{6+}/S_{tot} in the sample glasses (Metrich and Clocchiatti, 1996; Rowe et al., 2007; Rowe et al., 2009; Beermann et al., 2011). During the analysis using Δλ(SKα) of electron microprobe, significant changes of the S^{6+}/S_{tot} in the silicate glass have been observed (Rowe et al., 2007; Klimm et al., 2012), and it has also been well demonstrated that the S^{6+}/S_{tot} determined by Δλ(SKα) of electron microprobe is less precise than the S^{6+}/S_{tot} determined by sulfur K-edge XANES (Jugo et al., 2010). However, when the calibration of S^{6+}/S_{tot} vs. fO_2 was based on the S^{6+}/S_{tot} determined by Δλ(SKα) of electron microprobe, and if the sample fO_2 is above FMQ, the estimated fO_2 values should approach the actual values within 0.5 log units (Rowe et al., 2009; Beermann et al., 2011). Our measured high S^{6+}/S_{tot} values (0.68–0.91) for the basaltic samples (runs Cu02-1, Cu02-2, Cu05, Cu06, Cu07, Cu13, and Cu14) reveal that the sample fO_2 must be higher than FMQ + 1 (Table 2; Fig. S1). The fO_2 for the coexistence of Cu-bearing sulfide and anhydrite in natural andesitic to rhyolitic arc magmas is higher than FMQ + 1.5 (Parat et al., 2011; Chang and Audétat, 2018). Previous experimental studies also show that at 2–3 GPa and 1050 °C, the fO_2 that stabilizes coexisting pyrrhotite and anhydrite phases in rhyolitic to dacitic melts is ~FMQ + 2 (Jégo and Dasgupta, 2014; Li et al., 2019). We therefore concluded that the fO_2 of our experiments that were saturated with both anhydrite and sulfide should not be lower than FMQ + 1.5. For the samples which were not saturated with anhydrite because of the presence of a fluid phase, their fO_2 should not vary considerably relative to the fO_2 of the anhydrite-saturated samples. The measured S^{6+}/S_{tot} values (0.55–0.63) in andesitic to dacitic melts also imply that the fO_2 of these samples must be higher than FMQ + 1 (Table 2; Fig. S1). Accordingly, our experiments were overall under oxidized conditions (fO_2 > FMQ + 1 to FMQ + 1.5) corresponding to the fO_2 range required for the sulfide–sulfate transition in silicate melt and the oxidation state of typical arc magmas.

3.5. Partition coefficients

Nernst partition coefficients of Mn, Co, Cu, Zn, As, Se, Mo, Ag, Cd, Sn, Sb, Te, Re, Au, Pb, and Bi between crystalline MSS and silicate melt ($D^{MSS/SM}$), and between Cu-rich sulfide liquid and silicate melt ($D^{SL/SM}$), were calculated from their weight proportions in the related phases (Table 3). Fig. 2 shows $D^{SL/SM}$ as a function of the Cu content of the sulfide liquid. Figs. 3 and 4, and Figs. S2 and S3, show $D^{MSS/SM}$ and $D^{SL/SM}$ as a function of the content of total Fe oxides in the silicate melt, [FeO_{tot}]. $D^{SL/SM}$ range from 16 to 160 for Co, from 1100 to 8400 for Cu, from 50 to 220 for Se, from 1200 to 5900 for Ag, from 50 to 1800 for Cd, from 700 to 3300 for Te, from 15 to 510 for Re, from 5700 to 90,000 for Au, from 20 to 440 for Pb, and from 140 to 3300 for Bi. The $D^{SL/SM}$ for Mn, Zn, As, Mo, Sn, and Sb are below 1–40. $D^{MSS/SM}$ range from 55 to 260 for Co, from 530 to 1700 for Cu, from 74 to 110 for Se, from 30 to 110 for Ag, from 4 to 40 for Cd, from 15 to 70 for Te, from 200 to 5900 for Re, and from 140 to 270 for Au. The $D^{MSS/SM}$ for Mn, Zn, As, Mo, Sn, Sb, Pb, and Bi are below 1–3. In each individual experiment, Co, Re, and Mo partitioned preferentially into MSS relative to the sulfide liquid, whereas the other elements partitioned preferentially into the sulfide liquid. Under the presently investigated conditions, Cu, Au, Ag, Cd, Te, and Bi are strongly compatible in the sulfide liquid, Co, Se, Re, and Pb are moderately compatible in the sulfide liquid, and Mn, Zn, As, Mo, Sn, and Sb are incompatible to mildly compatible in the sulfide liquid. Whereas, Cu and Re are strongly compatible in MSS, Co, Se, Te, Ag, and Au are moderately compatible in MSS, and Mn, Zn, As, Cd, Mo, Sn, Sb, Pb, and Bi are incompatible to mildly compatible in MSS.

4. DISCUSSION

4.1. Parameters that affect sulfide/silicate melt partitioning of chalcophile elements

Fig. 2 shows that the $D^{SL/SM}$ of Co, Cu, Zn, As, Mo, Ag, Cd, Sn, Sb, Re, Te, Pb, and Bi is not significantly affected

Table 3
Partition coefficients (D) of trace elements between monosulfide solid solution (MSS), sulfide liquid (SL), and silicate melt (SM).

Exp. No		Mn	Co	Cu	Zn	As	Se	Mo	Ag	Cd	Sn	Sb	Te	Re	Au	Pb	Bi
Cu02-1	$D^{MSS/SM}$	0.4	55	533	0.6	0.05	95	0.4	30	5	<0.5	0.05	20	280	233	0.2	0.8
1-σ		0.0	2	54	0.1	0.02	11	0.0	8	1		0.02	2	11	59	0.1	0.2
Cu06	$D^{MSS/SM}$	0.3	57	644	0.6	<0.04	110	0.2	49	4	<0.3	0.0	25	197	165	0.1	1.0
1-σ		0.0	1	100	0.1		18	0.0	16	1		0.0	3	8	52	0.0	0.1
Cu08	$D^{MSS/SM}$	1.9	259	1063	2.9	2.1	82	1.3	53	42	<0.3	0.1	32	5928	200	0.3	2.6
1-σ		0.2	19	363	0.3	0.2	6	0.4	20	5		0.0	5	752	38	0.1	1.7
Cu10	$D^{MSS/SM}$	0.9	124	1204	1.6	0.1	74	1.7	107	16	<0.4	0.04	69	808	268	0.2	1.9
1-σ		0.0	5	106	0.1	0.0	16	0.1	7	2		0.02	35	48	54	0.1	0.3
Cu11	$D^{MSS/SM}$	1.0	188	1710	1.8	0.1	n.d	0.7	99	23	0.4	0.05	15	324	140	0.2	2.7
1-σ		0.2	32	399	0.5	0.0		0.2	23	5	0.1	0.02	1	99	9	0.1	1.1
Cu02-1	$D^{SL/SM}$	0.6	36	1754	2.2	0.8	185	0.3	1169	82	5.9	2.8	843	79	16,116	30	241
1-σ		0.0	1	214	0.1	0.1	21	0.1	305	10	0.5	0.6	125	5	4147	16	55
Cu02-2	$D^{SL/SM}$	0.4	24	1336	1.8	0.7	47	0.1	1248	68	6.4	2.4	1728	34	39,726	26	218
1-σ		0.1	2	125	0.1	0.1	29	0.0	301	9	1.0	0.5	1097	12	5222	4	48
Cu05	$D^{SL/SM}$	0.5	18	1267	1.6	0.7	160	0.2	1436	55	5.0	3.0	1623	33	18,023	24	178
1-σ		0.1	1	107	0.1	0.1	38	0.0	176	6	0.2	0.5	293	5	8402	3	29
Cu06	$D^{SL/SM}$	0.6	36	1905	2.2	0.6	221	0.2	1830	83	6.4	3.3	921	53	10,121	41	327
1-σ		0.0	1	114	0.1	0.0	39	0.1	170	7	0.9	0.1	131	8	1233	5	26
Cu07	$D^{SL/SM}$	0.3	17	1737	1.2	0.4	108	0.1	2034	56	3.3	1.7	1724	15	89,995	25	194
1-σ		0.0	1	70	0.2	0.1	18	0.0	158	4	0.1	0.0	276	3	26,290	3	9
Cu08	$D^{SL/SM}$	2.8	164	8450	19	18	210	0.2	5923	1767	39	17	1798	507	48,653	444	3358
1-σ		0.3	16	3218	4	2	32	0.1	2292	339	10	2	361	142	9471	138	2275
Cu09	$D^{SL/SM}$	1.0	63	1382	6.6	0.8	135	0.2	1490	475	9.6	3.2	2569	34	5718	80	777
1-σ		0.0	2	35	0.6	0.1	49	0.1	171	12	0.5	0.0	618	2	637	3	32
Cu10	$D^{SL/SM}$	1.6	90	2848	6.2	1.6	143	0.8	2401	306	12.9	5.0	2434	237	12,730	96	1090
1-σ		0.0	4	194	0.7	0.1	32	0.1	172	21	0.8	0.3	1216	18	2540	5	148
Cu11	$D^{SL/SM}$	1.7	96	6442	8.6	1.6	n.d	0.5	5393	565	19	7.2	709	70	12,125	173	1936
1-σ		0.3	16	1540	2.3	0.5		0.1	974	127	5	2.0	51	22	724	47	742
Cu12	$D^{SL/SM}$	0.8	44	1302	4.0	1.1	154	0.3	1722	232	8.3	3.4	3302	72	33,744	31	1091
1-σ		0.0	3	583	0.4	0.2	68	0.0	557	45	0.9	0.4	2221	28	2867	5	446
Cu13	$D^{SL/SM}$	0.4	20	1125	1.5	0.5	174	0.2	1393	54	5.1	2.2	742	34	34,846	31	208
1-σ		0.1	1	28	0.1	0.2	47	0.1	190	3	0.2	0.2	124	4	9031	4	27
Cu14	$D^{SL/SM}$	0.3	16	2054	1.2	0.3	104	0.1	1998	51	2.9	1.5	827	16	29,621	20	141
1-σ		0.0	1	210	0.0	0.1	2	0.0	442	3	0.1	0.2	154	1	2030	4	31
Cu15	$D^{SL/SM}$	1.2	82	5678	4.2	3.0	111	1.1	3768	443	12	3.5	3015	204	14,862	100	934
1-σ		0.1	14	201	0.1	1.0	26	0.1	455	55	2	1.4	1363	28	7497	27	412
Cu16	$D^{SL/SM}$	0.9	41	1247	3.4	0.8	143	0.3	1779	141	8	3.2	2464	54	10,359	60	623
1-σ		0.0	2	197	0.3	0.1	29	0.0	273	25	1	0.2	814	3	1522	8	105

n.d. not determined.

by the amount of Cu in the sulfide liquid over the investigated range of 2–45 wt.% Cu. This observation is consistent with the results of Kiseeva and Wood (2015) who showed that the presence of ~0.3–17 wt.% Cu in the sulfide liquid has a negligible effect on $D^{SL/SM}$ for a large number of chalcophile elements at temperatures of 1400–1700 °C. An exception is the $D^{SL/SM}$ for Au, which increase from 3700 to 90,000 with increasing the Cu content in the sulfide liquid (Fig. 2a). The presence of Cu in the sulfide liquid thus appears to favor the dissolution of Au. A previous study showed that Au solubility in Cu-rich sulfide (intermediate solid solution and bornite) is higher than in pyrrhotite under otherwise identical conditions (Fraley and Frank, 2014). The role played by Cu in the sulfide may be qualitatively consistent between this study and Fraley and Frank (2014).

Assuming an element M dissolves as M-oxide in the silicate melt, the partitioning of M between a sulfide phase and silicate melt can be described as:

$$MS_{x/2}(sulfide) + y/4O_2 = MO_{y/2}(SM) + x/4S_2 \quad (2)$$

where x and y refer to the average valence state of M in the sulfide and silicate melt, respectively. From the equilibrium constant (K) of Eq. (2), the following equation can be thermodynamically derived for describing the partitioning of M between a sulfide phase and silicate melt (Feng and Li, 2019):

$$logD_M^{sulfide/SM} = x/4logf_{S2} - y/4logf_{O2} + logK - log\frac{\gamma MS_{x/2}}{\gamma MO_{y/2}} + C \quad (3)$$

where $\gamma MS_{x/2}$ and $\gamma MO_{y/2}$are the activity coefficients of $MS_{x/2}$ and $MO_{y/2}$in the sulfide and silicate melt, respectively, and C is a constant. If M has a same valence state n in both sulfide and silicate, *i.e.*, $x = y = n$, and the activity of FeS in the sulfide is close to one, the FeO content in the silicate melt is a function of $-1/2(logfS_2 - logfO_2)$, and Eq. (3)

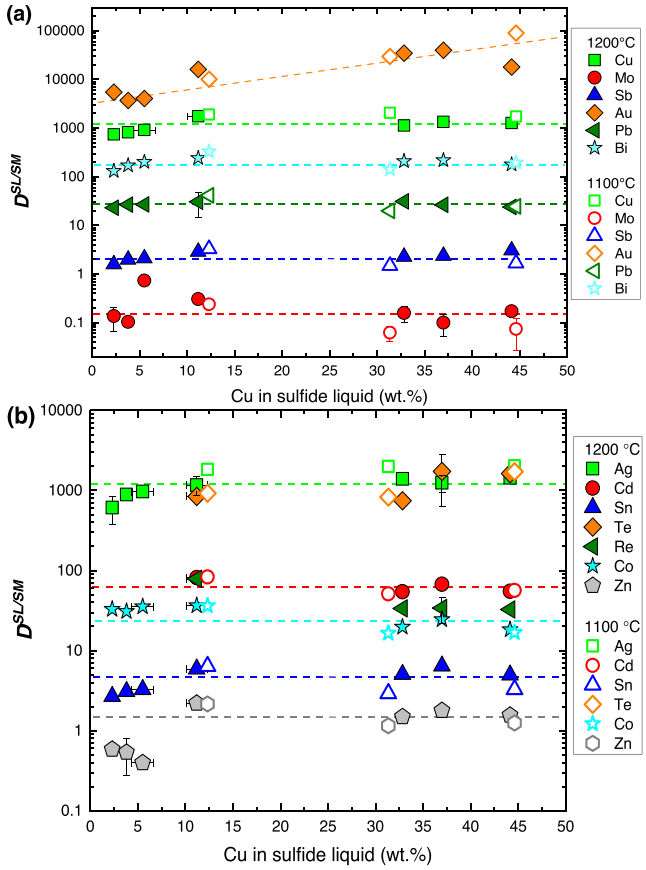

Fig. 2. Sulfide liquid/silicate melt partition coefficients ($D^{SL/SM}$) of chalcophile elements as a function of the Cu content in sulfide liquid. In (a), the $D^{SL/SM}$ of Cu, Mo, Sb, Au, Pb, and Bi are shown, and in (b) the $D^{SL/SM}$ of Ag, Cd, Sn, Te, Re, Co, and Zn are shown. Note that only $D^{SL/SM}_{Au}$ in (a) increases with increasing the Cu content in sulfide liquid, but the $D^{SL/SM}$ of other chalcophile elements remains nearly constant, as indicated by the dashed lines. The $D^{SL/SM}$ values were taken from runs Cu02-1, Cu02-2, Cu05, Cu13, Cu06, Cu07, and Cu14. Literature data from runs LY28, LY29, and LY31 in Li and Audétat (2012) were also plotted. Note that all the shown experiments had similar FeO_{tot} concentrations in the silicate melt and $fO_2 >$ FMQ.

can be written as below (Kiseeva and Wood, 2013; Feng and Li, 2019):

$$logD_M^{sulfide/SM} = -n/2\log[X_{FeO}] + C \quad (4)$$

where $[X_{FeO}]$ refers to the FeO content in the silicate melt, and C is a constant. In case of x≠y, *i.e.,* where two or more valence states of M are present in the silicate melt or sulfide, the following equation can be used to describe $D_M^{sulfide/SM}$ (Li and Audétat, 2015; Feng and Li, 2019):

$$logD_M^{sulfide/SM} = \mathrm{a}\cdot\log fO_2(\Delta FMQ) + \mathrm{b}\cdot\log[XFeO] \quad (5)$$

where a and b are coefficients. It has been found that the presence of O and Ni in the sulfide liquid could considerably affect $D_M^{sulfide/SM}$ (Kiseeva and Wood, 2013, 2015), although Cu has a very weak effect as discussed above. Following the approach of Kiseeva and Wood (2013, 2015) that was used to describe the effects of O, Ni, and Cu in the sulfide liquid on $D_M^{sulfide/SM}$, and also considering the effects of temperature and pressure, we obtain the following equation to describe $D_M^{sulfide/SM}$:

$$\begin{aligned} logD_M^{sulfide/SM} = {} & \mathrm{a}/\mathrm{T} + \mathrm{b}\cdot\mathrm{P}/\mathrm{T} + \mathrm{c}\cdot\log[X_{FeO_{tot}}]_{\mathrm{corr}} \\ & + \mathrm{d}\cdot\log fO2(\Delta FMQ) \\ & + \frac{1273}{\mathrm{T}}\cdot\left[\varepsilon_M^{FeO}\cdot\log(1-x_{FeO})\right. \\ & + \varepsilon_M^{NiS}\cdot\log(1-x_{NiS}) \\ & \left. + \varepsilon_M^{CuS_{0.5}}\cdot\log\left(1-x_{CuS_{0.5}}\right)\right] + \mathrm{C} \end{aligned} \quad (6)$$

where T is temperature in K; P is pressure in GPa; ε_M^{FeO}, ε_M^{NiS}, and $\varepsilon_M^{CuS_{0.5}}$ refer to non-ideal interaction between trace element M and matrix; x_{FeO}, x_{NiS}, and $x_{CuS_{0.5}}$ are mole fractions of FeO, NiS, and $CuS_{0.5}$ in the sulfide; and $[X_{FeO_{tot}}]_{\mathrm{corr}}$ is the total Fe oxides in the silicate melt corrected for the ideal activity of FeS in the sulfide as follows:

$$[X_{FeO_{tot}}]_{\mathrm{corr}} = [X_{FeO_{tot}}]/[Fe/(Fe+Ni+Cu)]_{sulfide} \quad (7)$$

It should be noted that if M dissolves as M-sulfide species, or as anions, in the silicate melt, $D_M^{sulfide/SM}$ does not follow Eqs. (4)–(6). Taking Au as an example, which dissolves dominantly as Au-sulfide species in the sulfide-saturated silicate melt, $D_{Au}^{sulfide/SM}$ can be described as (Li et al., 2019):

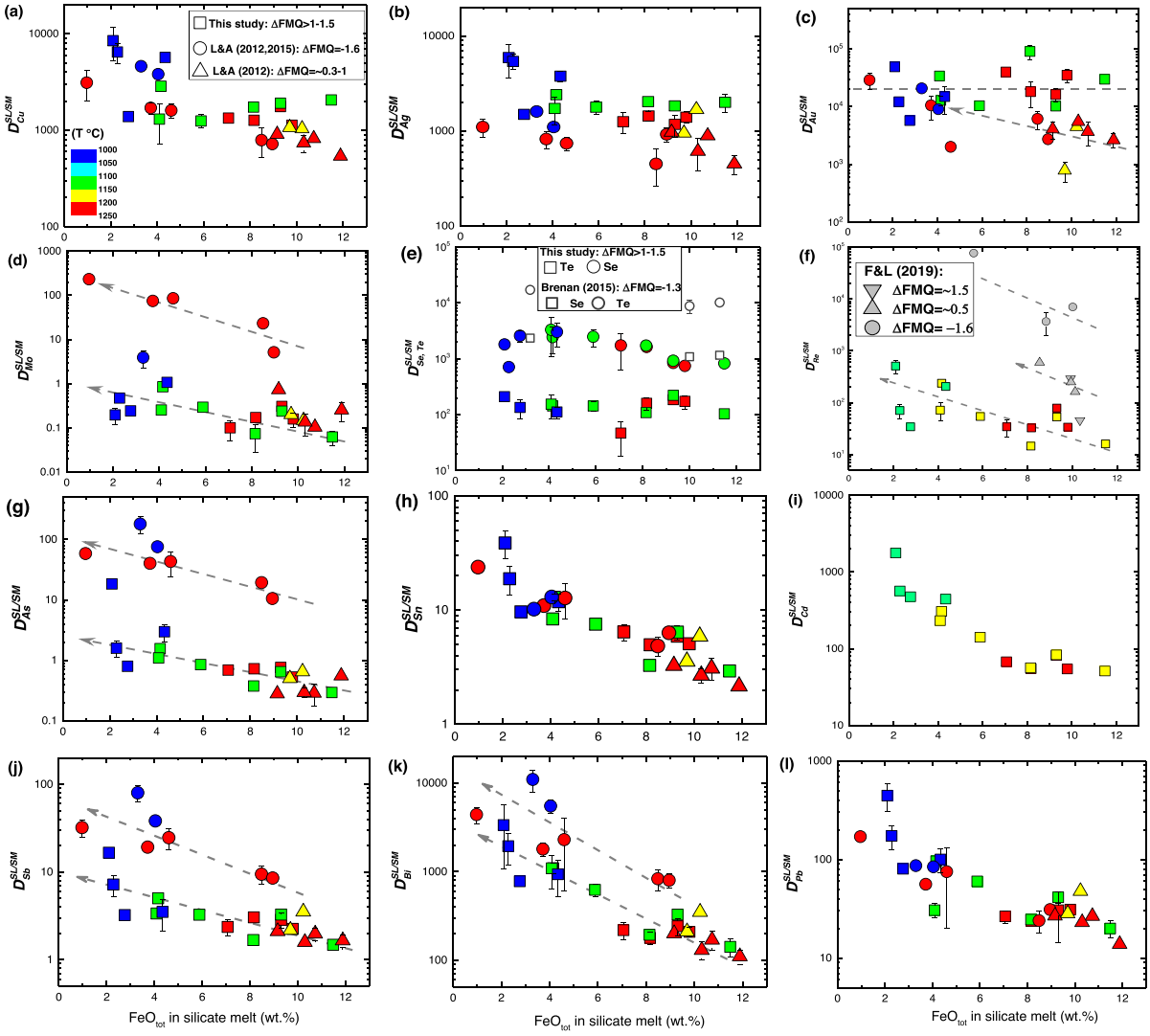

Fig. 3. Sulfide liquid/silicate melt partition coefficients of chalcophile elements ($D^{SL/SM}$) as a function of the FeO_{tot} content of the silicate melt. The data are color-coded for temperature. The arrow lines indicate the various evolution trends of $D^{SL/SM}$ versus FeO_{tot} because of the variation of fO_2. Note that $D^{SL/SM}$ for Mo, Se, Te, Re, As, Sb, and Bi decreases with increasing fO_2. Literature data were taken from Li and Audétat (2012, 2015), Brenan (2015), and Feng and Li (2019).

$$\log D_{Au}^{sulfide/SM} = A \cdot \log fS_2 - B \cdot \log[S, ppm]_{SM} + C \quad (8)$$

in which $[S, ppm]_{SM}$ is the content of reduced S in the sulfide-saturated silicate melt.

The presently determined $D^{SL/SM}$ and $D^{MSS/SM}$ values were plotted as a function of [FeO_{tot}] (Figs. 3 and 4; Figs. S2 and S3). The literature partitioning data obtained at similar temperatures were classified into two groups: one group obtained at fO_2 of ~FMQ-1.6 and the other group obtained at fO_2 of ~0.3–1 log units above FMQ. In this manner, we can distinguish the effect of fO_2 on $D^{SL/SM}$ and $D^{MSS/SM}$. The sparse $D^{MSS/SM}$ data for Cu, Ag, and Au (Simon et al., 2008; Botcharnikov et al., 2011; Zajacz et al., 2013; Botcharnikov et al., 2013), which have been discussed extensively in our recent studies (**Li and Audétat, 2012, 2013, 2015; Li et al., 2019) and are generally consistent with the present results, were not plotted for further comparison and discussion. Figs. 3 and 4, and Figs. S2 and S3, show that $D^{SL/SM}$ and $D^{MSS/SM}$ generally increase with decreasing [FeO_{tot}], but in a distinct manner for each element.

(1) The $D^{SL/SM}$ and $D^{MSS/SM}$ of Mn, Co, Zn, Cd, Sn, and Pb increase strongly with decreasing [FeO_{tot}], and the variation of $D^{SL/SM}$ and $D^{MSS/SM}$ at a given [FeO_{tot}] can be ascribed to the temperature variation. The sulfide/silicate melt partitioning behavior of Mn, Co, Zn, Cd, Sn, and Pb therefore follows Eq. (4) generally, because the valence states of these elements do not change with varying experimental conditions.

(2) At a given [FeO_{tot}], the $D^{SL/SM}$ and $D^{MSS/SM}$ of Re, Mo, As, Sb, and Bi vary by up to four orders of magnitude, with high fO_2 values causing low $D^{SL/SM}$ and $D^{MSS/SM}$ values. The fO_2-dependence of $D^{SL/SM}$ and $D^{MSS/SM}$ indicates that

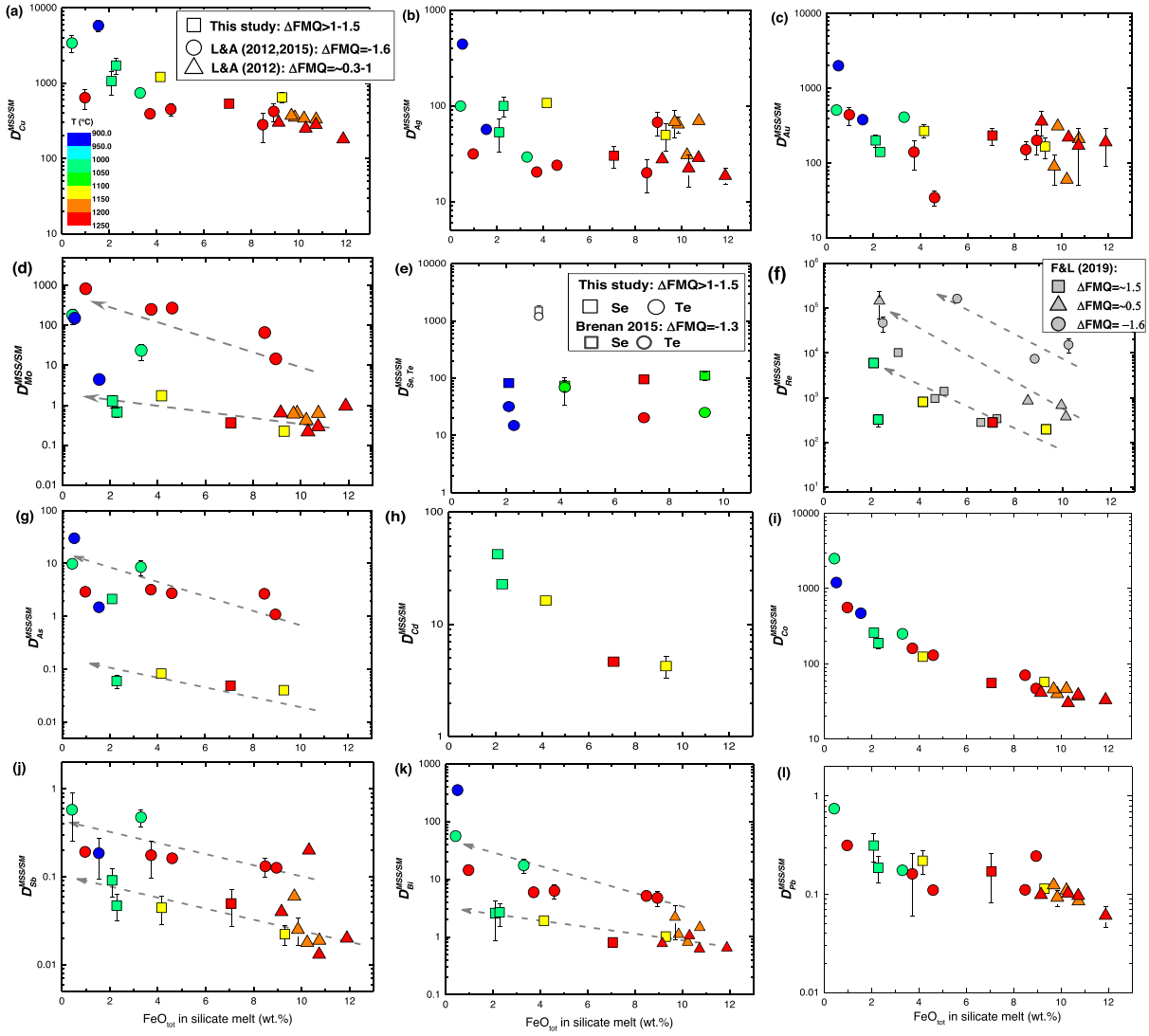

Fig. 4. MSS/silicate melt partition coefficients of chalcophile elements ($D^{MSS/SM}$) as a function of the FeO_{tot} content of the silicate melt. The data are color-coded for temperature. The arrows indicate different evolution trends of $D^{MSS/SM}$ vs. FeO_{tot} due to variations in fO_2. Note that the $D^{MSS/SM}$ of Mo, Se, Te, Re, As, Sb, and Bi decrease with increasing fO_2. Literature data were taken from Li and Audétat (2012, 2015), Brenan (2015), and Feng and Li (2019).

the valence states of Re, Mo, As, Sb, and Bi vary as a function of fO_2. The partitioning behavior of Re, Mo, As, Sb, and Bi thus follows Eq. (5) generally.

(3) The $D^{SL/SM}$ and $D^{MSS/SM}$ of Cu, Ag, and Au show a weak, or no, correlation with [FeO_{tot}]. Cu and Ag dissolve as both sulfide and oxide species in S^{2-}-bearing silicate melts (Zajacz et al., 2012; Zajacz et al., 2013; Lanzirotti et al., 2019). An additional complication arises from the fact that the relative proportion of Cu-sulfide and Cu-oxides species changes non-linearly with the S^{2-} content of the silicate melt (Lanzirotti et al., 2019). Lanzirotti et al. (2019) showed that more than 50% of Cu dissolves as Cu-sulfide species in basalts with >800 μg/g S^{2-}, but less than 30% of Cu dissolves as Cu-sulfide species in basalts with <600 μg/g S. How the Ag species changes with S^{2-} in the silicate melt remains unknown, but it may behave similarly as Cu. Therefore, the sulfide/silicate melt partitioning behavior of Cu and Ag may not be fully described by Eq. (4) or Eq. (5). The weak correlations between $D^{SL/SM}$, $D^{MSS/SM}$, and [FeO_{tot}] observed for Cu and Ag can be partly explained by the variation of the relative proportion of Cu-, and Ag-sulfide species in the silicate melt. In S^{2-}-rich silicate melt, Au forms mainly Au-sulfide species (Botcharnikov et al., 2011; Zajacz et al., 2013; Li and Audétat, 2013; Li et al., 2019), and a strong correlation between $D_{Au}^{MSS/SM}$ and reduced S in the silicate melt was found (Li et al., 2019). Accordingly, the $D^{SL/SM}$ and $D^{MSS/SM}$ of Au should not be expected to correlate with [FeO_{tot}] only, because the content of reduced S in sulfide-saturated silicate melt is a multiple function of P–T, silicate melt composition, silicate melt water content, and fO_2 (Jugo et al., 2010; Smythe et al., 2017). Therefore, all other

parameters, in addition to fS_2 as shown in Eq. (8), that affect the content of reduced S in the sulfide-saturated silicate melt, could potentially affect $D^{SL/SM}$ and $D^{MSS/SM}$ of Cu, Ag, and Au.

(4) The $D^{SL/SM}$ and $D^{MSS/SM}$ of Se and Te do not show considerable variation with [FeO_{tot}], and the $D^{SL/SM}$ and $D^{MSS/SM}$ values obtained in this study are much lower than those obtained at fO_2 of FMQ-1.3 by Brenan (2015). The valence states of Se and Te in silicate melts may change with fO_2, probably from Se^{2-} and Te^{2-} to Se^{4+}/Se^{6+} and Te^{4+}/Te^{6+} in a manner like S. Therefore, none of Eqs. (4)–(8) can sufficiently describe the sulfide/silicate melt partitioning behaviors of Se and Te, although increasing fO_2 decreases the $D^{SL/SM}$ and $D^{MSS/SM}$ of Se and Te.

In summary, we classified the elements Mn, Co, Cu, Zn, As, Se, Mo, Ag, Cd, Sn, Sb, Te, Re, Au, Pb, and Bi into four groups. Group-1 elements include Mn, Co, Zn, Cd, Sn, and Pb, the $D^{SL/SM}$ and $D^{MSS/SM}$ of which are mainly controlled by [FeO_{tot}]. The valence states of Group-1 elements appear to not change within the investigated fO_2 range of FMQ-1.6 to FMQ + 1.5. Group-2 elements include Re, Mo, As, Sb, and Bi, the $D^{SL/SM}$ and $D^{MSS/SM}$ of which are mainly controlled by [FeO_{tot}] and fO_2 because of changing element valence states. Group-3 elements include Cu, Ag, and Au, which dissolve as both sulfide and oxide species in silicate melts. Group-4 elements include Se and Te, which may dissolve as anions under reduced conditions but as cations under oxidized conditions.

To further understand quantitatively all parameters that potentially affect $D_M^{sulfide/SM}$, we have updated the parameterization of Li and Audétat (2015) and Kiseeva and Wood (2015) by fitting all available $D^{SL/SM}$ and $D^{MSS/SM}$ data into our Eq. (6) (Peach and Mathez, 1993; Gaetani and Grove, 1997; Brenan, 2008; Li and Audétat, 2012; Kiseeva and Wood, 2013; Zajacz et al., 2013; Mungall and Brenan, 2014; Kiseeva and Wood, 2015; Li and Audétat, 2015; Brenan, 2015; Feng and Li, 2019). The used $D^{SL/SM}$ and $D^{MSS/SM}$ data were obtained at 800 to 1700 °C, 1 bar to 3 GPa, and ~FMQ-3 to FMQ + 1.5; the silicate melts contain 0.1–40 wt.% FeO and the sulfides contain 0–45 wt.% Cu, 0–59 wt.% Ni, and up to 10 wt.% O. The obtained fitting coefficients are tabulated in Table 4. Note that, since the content of reduced S in the silicate melt is not known, we do not consider the effect of reduced S in the silicate melt when fitting $D^{SL/SM}$ and $D^{MSS/SM}$ for Cu and Ag. The $D^{MSS/SM}$ of Au, and probably the $D^{SL/SM}$ of Au as well, depend more strongly on the content of reduced S in the silicate melt, as indicated by Eq. (8). The parameterization of Li et al. (2019) for Au is thus not updated using the present data obtained under both anhydrite- and sulfide-saturated conditions. In addition, [FeO_{tot}] is not corrected when fitting $D^{MSS/SM}$, because MSS usually contain only a few wt.% Cu and Ni, and we do not find any considerable difference in the obtained fitting coefficients when fitting $D^{MSS/SM}$ with or without correcting [FeO_{tot}]. Furthermore, a fO_2 value of FMQ + 1.5 was used for all experiments in this study. The obtained fitting coefficients (Table 4) indicate that the $D^{MSS/SM}$ and $D^{SL/SM}$ of many elements, such as Co, Ni, Cu, and Ag, decrease with increasing temperature. However, temperature has an opposite role for the $D^{SL/SM}$ of Mn and Zn. There is a large uncertainty in the effect of temperature on the $D^{MSS/SM}$ of Ag, Sn, Cd, As, Mo, and Re, and on the $D^{SL/SM}$ of As, Re, and Mo. In Table 4, the temperature effect was thus not considered for the $D^{MSS/SM}$ and $D^{SL/SM}$ of Re and Mo, although Li and Audétat (2015) and Feng and Li (2019) suggested a positive effect of temperature on the $D^{MSS/SM}$ and $D^{SL/SM}$ of Mo. The $D^{SL/SM}$ of Co, Ni, Zn, Ag, Sn, and Cd decrease with increasing pressure, but the $D^{SL/SM}$ of Re appear to increase with increasing pressure. The presence of Ni in the sulfide is considerably important for the $D^{MSS/SM}$ and $D^{SL/SM}$ of many elements, but the effect of Cu is negligible for most of the elements. We suggest that Eq. (6) together with the fitting coefficients listed in Table 4 can be used to predict $D^{MSS/SM}$ and $D^{SL/SM}$ of chalcophile elements in magmas at the shallow upper mantle to crust conditions. However, to fully describe $D^{SL/SM}$ or $D^{MSS/SM}$ for each of the above trace elements, in particular those from Group-3 to Group-4, future work is needed to investigate the effect of each single parameter on $D^{SL/SM}$ and $D^{MSS/SM}$ and parameterize $D^{SL/SM}$ and $D^{MSS/SM}$ as a multiple function of all relevant parameters.

4.2. Magmatic fractionation of chalcophile elements

A shown above, the $D^{SL/SM}$ of certain elements are rather different from the corresponding $D^{MSS/SM}$, hence specific chalcophile element ratios can be used to identify which sulfide phase(s) segregated during magmatic differentiation, and at which fO_2 conditions this happened. Fig. 5 shows the variation of several partition coefficient ratios as a function of [FeO_{tot}]. The $D_{Cu}^{SL/SM}/D_{Ag}^{SL/SM}$ ratio remains nearly constant at ~1 under oxidized conditions (Fig. 5a). Under reduced conditions, the $D_{Cu}^{SL/SM}/D_{Ag}^{SL/SM}$ ratio appears to increase slightly with decreasing [FeO_{tot}] at <4 wt.% [FeO_{tot}], but it is always below 4. Thus, saturation and segregation of sulfide liquid does not significantly change the Cu/Ag ratio in the residual magma. However, the $D_{Cu}^{MSS/SM}/D_{Ag}^{MSS/SM}$ ratio is significantly larger than 5 and increases up to 100 with decreasing [FeO_{tot}] (Fig. 5a). Therefore, saturation and segregation of MSS can cause a significant Cu–Ag fractionation in the residual magma. The $D_{Cu}^{SL/SM}/D_{Se}^{SL/SM}$ and $D_{Cu}^{MSS/SM}/D_{Se}^{MSS/SM}$ ratios are between 6 and 60 under oxidized conditions, but they are below unity under reduced conditions (Fig. 5b). Therefore, saturation and segregation of sulfides at different redox states can cause contrasting Cu–Se fractionations in the residual magma. Fig. 5c shows a similarly strong effect of fO_2 on the Cu–Mo fractionation in magma, and the $D_{Cu}^{SL/SM}/D_{Mo}^{SL/SM}$ and $D_{Cu}^{MSS/SM}/D_{Mo}^{MSS/SM}$ ratios can be up to 10^5 under oxidized conditions. The $D_{Au}^{SL/SM}/D_{Cu}^{SL/SM}$ ratio is 1–60 but the $D_{Au}^{MSS/SM}/D_{Cu}^{MSS/SM}$ ratio is 0.04–1 (Fig. 5d). Therefore, as has been shown previously (Li and Audétat,

Table 4
Fitting coefficients obtained for Eq. (6)[¥].

	No. of data (n)	a	1σ	b	1σ	c	1σ	d	1σ	ε^{FeO}	1σ	ε^{NiS}	1σ	$\varepsilon^{CuS0.5}$	1σ	C	1σ	R^2	[#]SEE (σ)
***D*$^{SL/SM}$**																			
Mn	n = 90	−2110	219	−178	35	−1.10	0.06			−3.20	0.45	1.30	0.22	−1.30	0.19	2.25	0.15	0.92	0.10
Co	n = 80	460	210	−133	60	−0.99	0.06			0.76	0.45	−0.67	0.23	0.60	0.20	2.54	0.15	0.93	0.09
Cu	n = 128	4745	228	Insign.		−0.43	0.06			3.37	0.51	0.50	0.26	Insign.		0.36	0.16	0.85	0.15
Ni	n = 91	2969	445	−325	52	−0.94	0.06			Insign.		Insign.		Insign.		2.34	0.27	0.78	0.19
Zn	n = 79	−1967	269	−553	76	−1.13	0.08			−1.74	0.58	0.75	0.29	−1.15	0.25	3.06	0.19	0.90	0.11
Ag	n = 80	3559	254	−162	75	−0.17	0.07			3.84	0.54	1.05	0.31	Insign.		1.02	0.19	0.86	0.13
Sn	n = 31	Insign.		−227	80	−0.84	0.09			Insign.		1.25	0.76	Insign.		1.88	0.09	0.85	0.11
Cd	n = 62	1679	308	−439	130	−0.99	0.04			Insign.		0.43	0.22	−0.42	0.20	2.14	0.25	0.94	0.09
Pb	n = 88	483	237	−159	65	−1.04	0.04			Insign.		0.30	0.24	−0.33	0.18	2.42	0.17	0.89	0.11
Sb	n = 39	2741	987	Insign.		−0.66	0.13	−0.23	0.03	4.24	2.14	Insign.		Insign.		−0.39	0.76	0.82	0.18
Re	n = 36	Insign.		331	179	−1.29	0.29	−0.69	0.06	Insign.		Insign.		Insign.		4.00	0.31	0.81	0.37
As	n = 30	5864	2050	Insign.		−1.03	0.30	−0.45	0.06	Insign.		Insign.		Insign.		−2.66	1.62	0.82	0.32
Mo	n = 38	Insign.		Insign.		−1.42	0.30	−0.57	0.07	Insign.		6.50	3.00	Insign.		1.74	0.31	0.80	0.40
Bi	n = 31	6202	1043	Insign.		−0.93	0.15	−0.18	0.03	5.68	2.82	Insign.		Insign.		−0.51	0.84	0.89	0.17
***D*$^{MSS/SM}$**																			
Mn	n = 32	1299	569	Insign.		−0.90	0.06					6.43	1.34	Insign.		−0.45	0.43	0.95	0.11
Co	n = 32	2134	484	Insign.		−1.00	0.05					Insign.		Insign.		1.20	0.36	0.95	0.10
Cu	n = 52	2260	484	Insign.		−0.69	0.06					Insign.		Insign.		1.64	0.38	0.86	0.15
Ni	n = 24	3872	916	Insign.		−1.06	0.18					6.19	2.63	Insign.		1.39	0.66	0.88	0.14
Zn	n = 31	Insign.		−228	83	−1.27	0.07					Insign.		Insign.		1.00	0.06	0.95	0.12
Ag	n = 33	1969	973	Insign.		−0.42	0.12					−6.43	2.61	Insign.		0.40	0.77	0.54	0.23
Sn	n = 10	−5483	3382	Insign.		−1.41	0.25					Insign.		Insign.		4.06	2.54	0.80	0.30
Cd	n = 5	−3015	1808	Insign.		−1.69	0.25					Insign.		Insign.		4.41	1.49	0.97	0.04
Pb	n = 31	Insign.		Insign.		−0.63	0.07					Insign.		Insign.		−0.38	0.06	0.71	0.16
As	n = 17	5465	2643	Insign.		−0.36	0.23	−0.51	0.07			17.31	5.73	Insign.		−3.80	2.00	0.84	0.30
Mo	n = 37	Insign.		Insign.		−0.88	0.21	−0.51	0.05			11.50	5.00	Insign.		1.50	0.17	0.81	0.43
Sb	n = 21	Insign.		Insign.		−1.00	0.16	−0.23	0.05			Insign.		Insign.		−0.44	0.13	0.76	0.32
Re	n = 18	Insign.		Insign.		−2.00	0.10	−0.56	0.10			Insign.		Insign.		5.20	0.40	0.70	0.48
Bi	n = 24	4283	1080	Insign.		−0.40	0.10	−0.26	0.03			Insign.		Insign.		−2.34	0.81	0.91	0.15

1σ is the standard deviation of each coefficient reported.
R^2 is the correlation coefficient, which provides a measure of how well the observed results are reproduced by the equation.
¥ For the equation of the form $\log(D^{SL/SM}, D^{MSS/SM}) = C + a/T + b\cdot P/T + c\cdot\log[FeO_{tot}] + d\cdot\Delta FMQ + 1273/T \cdot[\varepsilon^{FeO}\cdot\log(1\text{-}X_{FeO}) + \varepsilon^{NiS}\cdot\log(1\text{-}X_{NiS}) + \varepsilon^{CuS0.5}\cdot\log(1\text{-}X_{CuS0.5})]$,
where T is temperature in K, P is pressure in GPa, and X referes to mole fraction, and $[FeO_{tot}]$ is the total Fe oxides in the silicate melt in wt.%.
For $\log(D^{SL/SM})$ in Eq. (6), $[FeO_{tot}]$ is corrected for ideal activity of FeS in the sulfide (see the main text).
Insign. means the coefficient has an uncertainty significnalty larger than 50%, and we consider the effect of the assocated parameter is insignificant.
[#] SEE = Standard error of estimates.

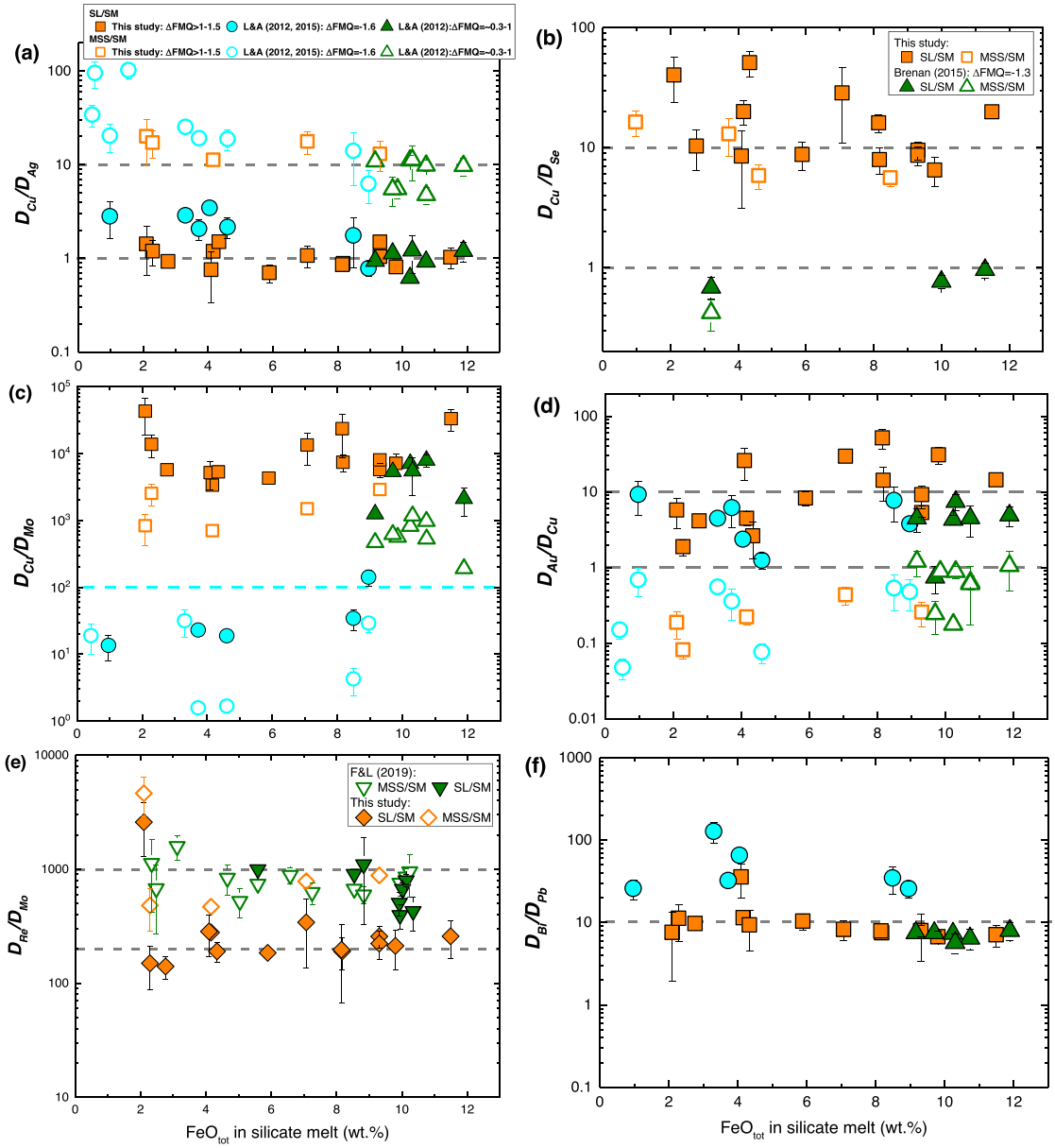

Fig. 5. Ratio of various sulfide/silicate melt partition coefficients as a function of the FeO_{tot} content in silicate melt. (a) $D_{Cu}^{SL/SM}/D_{Ag}^{SL/SM}$ is nearly constant at a value of 1, but $D_{Cu}^{MSS/SM}/D_{Ag}^{MSS/SM}$ is always higher than 5 and increases with decreasing the FeO_{tot} content of the silicate melt. (b) D_{Cu}/D_{Se} is below 1 under reduced conditions, but $\geq$5 under oxidized conditions. (c) D_{Cu}/D_{Mo} is below 100 under reduced conditions, but up to 10^5 under oxidized conditions. (d) $D_{Au}^{SL/SM}/D_{Cu}^{SL/SM}$ is 1–70 whereas $D_{Au}^{MSS/SM}/D_{Cu}^{MSS/SM}$ is 0.04–1. (e) D_{Re}/D_{Mo} remains constant for both SL and MSS and is higher than 100 under all investigated conditions. (f) $D_{Bi}^{SL/SM}/D_{Pb}^{SL/SM}$ is about 10 under oxidized conditions, but increases to 30–100 under reduced conditions.

2012), the Cu/Au ratio in the residual magma is strongly controlled by the type of segregating sulfide phase. Although the $D^{SL/SM}$ and $D^{MSS/SM}$ for Re and Mo are strongly controlled by fO_2 (Fig. 3d and f; Fig. 4d and f), the $D_{Re}^{SL/SM}/D_{Mo}^{SL/SM}$ and $D_{Re}^{MSS/SM}/D_{Mo}^{MSS/SM}$ ratios appear to be constant values of ~200–800 (Fig. 5e). Therefore, the Re/Mo ratio decreases in the residual magma if any sulfide phase is segregated, but particularly so if the sulfide phase is MSS. Under oxidized conditions the $D_{Bi}^{SL/SM}/D_{Pb}^{SL/SM}$ ratio is constant at ~10, but it increases to 100 under reduced conditions (Fig. 5f). The saturation and segregation of sulfide liquid from reduced magmas can thus cause significant Bi–Pb fractionation. In summary, magmatic fractionations between Cu, Ag, Mo, Se, Re, Au, Pb, and Bi are controlled not only by the type of segregating sulfide phase, but also by the fO_2 conditions under which the sulfides saturate and segregate.

4.3. Sulfide phase relations during arc magma differentiation

Nearly all arc magmas reach sulfide saturation at some point during their evolution (*e.g.*, Lee et al., 2012; Chang

and Audétat, 2018; Jenner et al., 2010; Williams et al., 2018). The saturating sulfide phase has been suggested to be sulfide liquid or Cu-rich crystalline sulfide in the case of the back-arc magmas of the Eastern Manus Basin (Jenner et al., 2010; Park et al., 2013). However, based on the observation that Cu is more depleted than Ag and Au in the evolved back-arc magmas, it has been suggested that MSS was the main sulfide phase (Li and Audétat, 2012; Li, 2014a). Furthermore, based on the observation that the continental crust is depleted in Cu, less depleted in Au, and slightly enriched in Ag, compared to the global average MORB, Li and Audétat (2013) proposed that the main sulfide phase that segregated during the formation of the continental crust was MSS, which view is also supported by the study of Wang et al. (2018).

The present experiments can be used to place further constrains on the nature of the sulfide phase segregating during arc magma differentiation. Whether the sulfide phase exsolved from arc magmas occurs as MSS or sulfide liquid depends not only on *P*–*T* but also on the Cu content in the sulfide phase, which in turn depends on the Cu content of the arc magma. Fig. 6 shows that at temperatures of 1000–1200 °C the Fe–Cu–S sulfide occurs in the form of MSS if the Cu content is not higher than 5 wt.%, whereas it occurs as sulfide liquid if the Cu content is higher than 11 wt.%. Fig. 6 also shows that the silicate melts that contain more than 100 μg/g Cu are saturated with Cu-rich sulfide liquid only, whereas the silicate melts that contain 30–70 μg/g Cu are saturated with both MSS and Cu-rich sulfide liquid. At even lower Cu concentrations (the threshold value being unconstrained), only MSS precipitates. These observations imply that sulfides that exsolve from basaltic to dacitic arc magmas with >100 μg/g Cu should be Cu-rich sulfide liquid, whereas the sulfides exsolving from basaltic to dacitic arc magmas with 30–70 μg/g Cu should be coexisting MSS and Cu-rich sulfide liquid.

In unaltered rocks from island arcs with crustal thicknesses of <20 km, Cu first increases from ~50–120 μg/g in basalts to a maximum of ~110–210 μg/g in magmas with ~4.3 wt.% MgO, but then drops to ~30–90 μg/g at ~3 wt.% MgO (Chiaradia, 2014). However, in continental arcs with crustal thicknesses of >30 km, Cu decreases directly from ~36–80 μg/g in basalts to ~15–35 μg/g in magmas with ~3 wt.% MgO. The drop of Cu in magmas at ~4.3 wt.% MgO in the island arcs, and the direct decrease of Cu in magmas in continental arcs, are ascribed to sulfide saturation (Chiaradia, 2014). According to Fig. 6, the precipitating sulfide phase should have been coexisting MSS and Cu-rich sulfide liquid in island arcs, and it should have been mainly MSS in continental arcs. The present experimental temperatures (1000–1200 °C) match well the arc magmatic differentiation temperatures; however, the experimental pressures (0.5–1 GPa) are generally lower than the arc magmatic differentiation pressures, in particular for continental arcs. This is because arc magma differentiation takes place mainly in a hot zone at the root of the crust (Annen et al., 2006). High pressure favors the stabilization of MSS under otherwise equivalent conditions (Li and Audétat, 2012, 2013). Accordingly, it has been concluded that during magmatic differentiation in continental arcs MSS is the dominant sulfide phase. These inferences are supported by available observations on natural arc magmatic rocks (Hattori, 1993; Agangi and Reddy, 2016; Chang and Audétat, 2018; Georgatou et al., 2018). For example, in the Sunda arc of Indonesia, Cu reaches ~250–300 μg/g in arc magmas with ~4 wt.% MgO, but then it drops abruptly to below 50 μg/g as soon as saturation in a Cu-rich sulfide liquid was reached (Agangi and Reddy, 2016). In contrast, Chen et al. (2020) found that during magmatic differentiation in the deep continental arc of Arizona, the precipitating sulfide phase in garnet-pyroxenite cumulates was dominantly MSS. Chang and Audétat (2018) also found a dominant presence of MSS over sulfide liquid in cumulate xenoliths from the Santa Rita and Cerrillos continental-arc magma systems in New Mexico (USA).

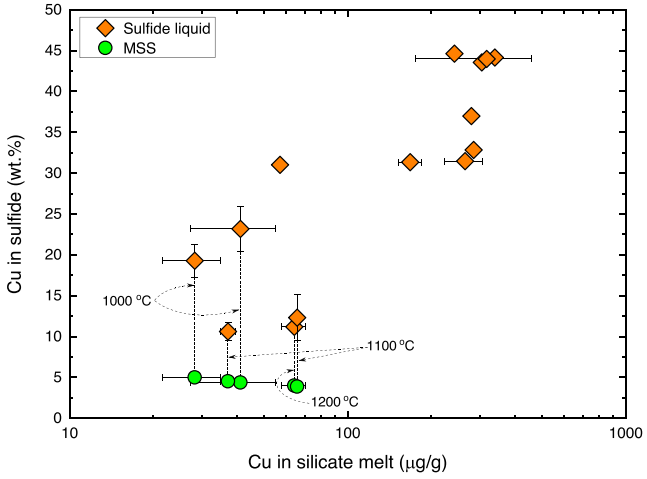

Fig. 6. Type of precipitating Fe–Cu–S sulfide as a function of the Cu content of the silicate melt. This figure shows that when the Cu content of the silicate melt is above ~100 μg/g, the precipitating sulfide is a Cu-rich sulfide liquid, whereas when the Cu content is between 30 and 70 μg/g, both MSS and Cu-rich sulfide liquid precipitate. The dashed lines connect pairs of coexisting crystalline MSS and Cu-rich sulfide liquid in individual experiments. The experimental pressures are 0.5–1 GPa and temperatures are 1000–1200 °C, and the experimental fO_2 values are above FMQ + 1 to FMQ + 1.5.

4.4. The fate of chalcophile elements in arc magmas and the formation of continental crust

Since arc magmatism is ultimately related to the formation of Earth's continental crust (Hawkesworth et al., 2010; Jagoutz and Kelemen, 2015; Rudnick, 1995), we focus on the fate of chalcophile elements during arc magmatic differentiation in order to constrain the formation conditions of Earth's continental crust. Most of the chalcophile elements are incompatible in common silicate and oxide minerals (Mallmann and O'Neill, 2007; Li, 2014b; Leitzke et al., 2017), and as mentioned above, sulfide saturation is almost inevitable in evolved arc magmas. We used the sulfide/silicate melt partitioning data presented in Figs. 3 and 4 and as described by Eq. (6), and a differentiation model described below, to predict the evolution trends of several typical chalcophile elements during arc magmatic differentiation. For this purpose, we first compiled a global dataset from GEOROC (http://georoc.mpch-mainz.gwdg.de/georoc/Entry.html), using the same approach as used by Chiaradia (2014), in order to obtain the major element contents (median values) of arc basalts to rhyolites at arcs with a crustal thickness of >30 km and at arcs with a crustal thickness of <20 km. The compiled dataset is given in Table S5. The corresponding Cu contents in global arc magmas were taken from Chiaradia (2014). The water content in the parental basalt was set to 1.5 wt.% and water was assumed to be perfectly incompatible during crystallization. The magmatic differentiation pressure was set to 1 GPa for arcs with a crustal thickness of >30 km, and 0.3 GPa for arcs with a crustal thickness of <20 km. The degree of crystallization (F) and magma temperature were calculated using the correlations between silicate melt SiO_2 content, T, and F, calibrated by Chang and Audétat (2018) using experimental data obtained at 0.4–1.3 GPa. The liquidus temperatures of the arc basalts to rhyolites were also calculated using MELTS (Ghiorso et al., 2002). We used the SCSS model of Smythe et al. (2017) to determine the S content of the silicate melt, and then used the change of SCSS in the silicate melt at each step of crystallization to determine the mass of S precipitated as Fe–Cu–Ni–O–S sulfide. In the Fe–Cu–Ni–O–S sulfide, the Ni content was fixed at 2 wt.% considering that the Ni conents of sulfides in arc magmatic rocks are rather low (Chang and Audétat, 2018; Georgatou et al., 2018), the O content was calcualted using the FeO_{tot} content of the arc magmas when the Fe–Cu–Ni–O–S sulfide is sulfide liquid (Kiseeva and Wood, 2015), and the Cu content was calcualted using the partitioning of Cu between sulfide and silicate melt by an iterative appoach. When the Fe–Cu–Ni–O–S sulfide is MSS, the O conent in the sulfide was not considered. The mass of precipitating sulfides at each step of crystallization does not much depend on the initial water content or magma temperature. Both a fractional and an equilibrium crystallization model, and both MSS and sulfide liquid, were considered during arc magmatic differentiation, and perfect incompatibility of Cu, Ag, As, Sn, Sb, Re, Mo, Pb, Bi in silicate and oxide minerals were assumed (Mallmann and O'Neill, 2007; Li, 2014b; Leitzke et al., 2017). The used $D^{SL/SM}$ and $D^{MSS/SM}$ of Cu, Ag, As, Sn, Sb, Re, Mo, Pb, and Bi were calculated using Eq. (6) and the associated fitting coefficients given in Table 4. The used $D^{SL/SM}$ and $D^{MSS/SM}$ of Se are 200 and 100, respectively, at fO_2 > FMQ + 1 to FMQ + 1.5, and 1500 and 1200, respectively, at fO_2 of FMQ-1.3 (Brenan, 2015). The used $D^{MSS/SM}$ of Au was varied from 200 to 500 with magma differentiation (Fig. 4c), and the used $D^{SL/SM}$ of Au was fixed at 10,000 (Fig. 3c). To model the chalcophile elements of variable valence states, the fO_2 of the arc magmas was varied from ~FMQ-1.3 to FMQ + 1.5, with the effects of magmatic degassing and/or crystallization on fO_2 (Jenner et al., 2010) not considered.

Fig. 7a and b show that when the crustal thickness is >30 km, the Cu content of arc magmas decreases with decreasing MgO dure to sulfide saturation. In contrast, when the crustal thickness is <20 km, the Cu content first increases with decreasing MgO due to sulfide undersaturation, and then starts to decrease at ~4.3 wt.% MgO due to sulfide saturation (Fig. 7c). Since the behavior of Cu in arc magmas depends on the nature of the precipitating sulfide phase(s), we tested which phase(s) best reproduce(s) the Cu evolution trends recorded in natural arc magmas. Fig. 7a shows that if the precipitating sulfides are dominantly MSS, our model reproduces well the Cu evolution trend shown by arcs with a crustal thickness of >30 km, while already the presence of 20% sulfide liquid leads to distinctly lower trends than those observed. For Honshu, Cascades, and the Central Andes arcs, the mass of sulfides precipitated at >4 wt.% MgO needs to be only about half of that calculated based on the SCSS variation during crystallization (Fig. 7b). This could be due to the oxidization of those arc magmas during early differentiation, which suppresses the mass of precipitating sulfides. Fig. 7c shows that in order to reproduce the Cu evolution trend in arcs with a crustal thickness of <20 km, the precipitating sulfides at <~4.3 wt.% MgO need to be a mixture of MSS and sulfide liquid, with the mass proportion of sulfide liquid ranging from 50% up to 90%. It is worth noting that if a fraction of S^{6+} is converted into S^{2-} and precipitated as sulfides during magmatic differentiation at continental arcs, the proportion of MSS in the precipitating sulfides would increase; if a fraction of S^{2-} is degassed during magmatic differentiation at island arcs, then the proportion of sulfide liquid in the precipitating sulfides would increase.

Using the same models that successfully reproduce the Cu evolution trends in the investigated arc magmas (Fig. 7), and also considering the effect of fO_2 (ΔFMQ = −1.3 to 1.5) on $D^{SL/SM}$ and $D^{MSS/SM}$ for Se, Sn, As, Bi, Re, and Mo, we predicted the evolutionary trends of Ag, Au, Re, Se, Pb, Bi, Mo, As, Sn, and Sb (Fig. 8). The initial concentrations of these elements in the arc basalts (75 μg/g Cu, 38 ng/g Ag, 3.8 ng/g Au, 5 μg/g Pb, 0.015 μg/g Bi, 0.13 μg/g Se, 0.15 μg/g Sb, 1 μg/g Sn, 0.5 μg/g Mo, 1.1 μg/g As, 0.5–1.5 ng/g Re) were taken from (Sun et al., 2003; Jenner et al., 2010; Jenner et al., 2012; Park et al., 2013; Cox et al., 2019). Fig. 8 shows the predicted results for arcs with a crustal thickness of >30 km, from which it can be seen that when the precipitating sulfides are pure MSS, Ag, Se, and Bi behave incompatibly and become

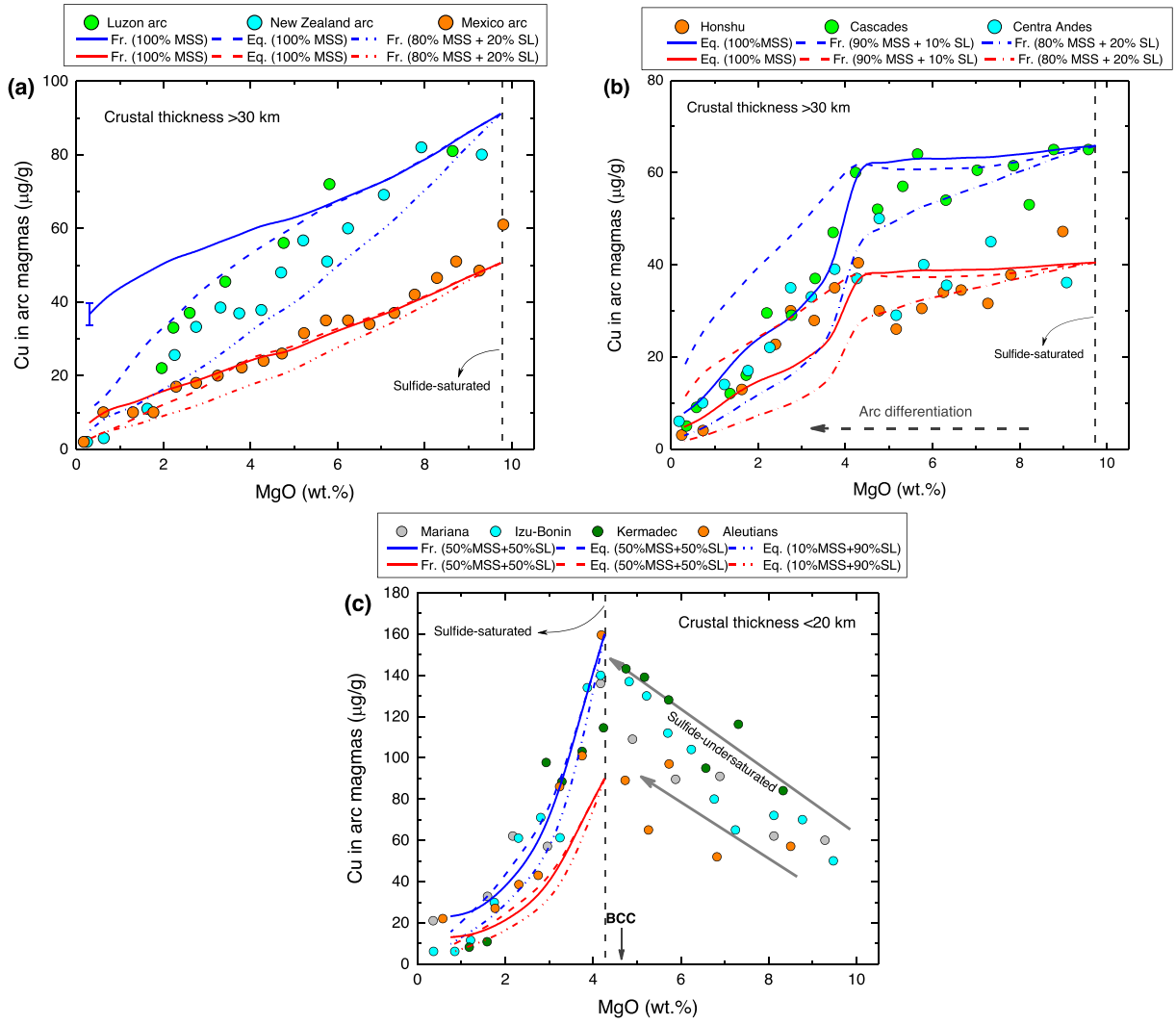

Fig. 7. Observed vs. modeled Cu evolution trends in arc magmas. (a) The trends displayed by the Luzon, New Zealand, and the Mexico arc can be reproduced with an initial Cu content of 50–100 μg/g in the basalt, and with the precipitating sulfide being dominated by MSS (i.e., less than 20% sulfide liquid). (b) The trends displayed by the Honshu, Cascades, and the Central Andes arc can be reproduced with an initial Cu content of 40–65 μg/g in the basalt, and with the mass of precipitating sulfides at >4 wt.% MgO being only about half of that in (a). (c) The trends displayed by the Mariana, Izu-Bonin, Kermadec, and the Aleutians arc can be reproduced with an initial Cu content of 90–160 μg/g in the arc magmas when sulfide saturation occurs at ~4.3 wt.% MgO, and with 50–90% of the precipitating sulfide being sulfide liquid. Note that in (a) and (b), the crustal thickness is >30 km and sulfide saturation occurred at the beginning of magmatic differentiation, whereas, in (c) the crustal thickness is <20 km and sulfide saturation occurred at ~4.3 wt.% MgO. In the model calculations, both fractional (Fr.) and equilibrium (Eq.) segregation of the precipitating sulfides, and both MSS and sulfide liquid, were considered. See the main text for details of the setup of the model. BCC denotes Earth's bulk continental crust. The error bar shown in (a) is the typical error (±3 ppm) of the calculated Cu contents in arc magmas, based on the standard deviation of the fitting (Table 4).

enriched in the residual magmas under oxidized conditions (ΔFMQ = 1–1.5). However, the occurrence of 10–20% sulfide liquid, relative to the total mass of sulfides precipitated, would dramatically deplete the residual magmas in Au (Fig. 8a). Under oxidized conditions (ΔFMQ = 1), Re decreases moderately with decreasing the MgO content in arc magmas, but drops abruptly at fO_2 of FMQ-1 to FMQ (Fig. 8b). Under reduced conditions (ΔFMQ = −1.3 to −1), Se and Bi would also be depleted in the residual magmas (Fig. 8c and d). In contrast, Mo always behaves as an incomptabile element and get enriched in the residual magmas (Fig. 8d). As, Sn, and Pb behavior similarly as Mo mainly due to their low values of $D^{SL/SM}$ and $D^{MSS/SM}$. Fig. 8e shows the predicted results for arcs with a crustal thickness of <20 km. It can be seen from Fig. 8e that all chalcophile elements including Ag, Au, Re, Se, Cu would get enriched and not fractionated in magmas at >~4.3 wt.% MgO because of sulfide-undersaturation. However, the magmas at ≤~4.3 wt.% MgO are saturated with sulfides, and Ag, Au, and Re in the magmas drop significantly.

Fig. 8 also shows the comparisons of our predicted results with the data obtained from natural arc/back-arc

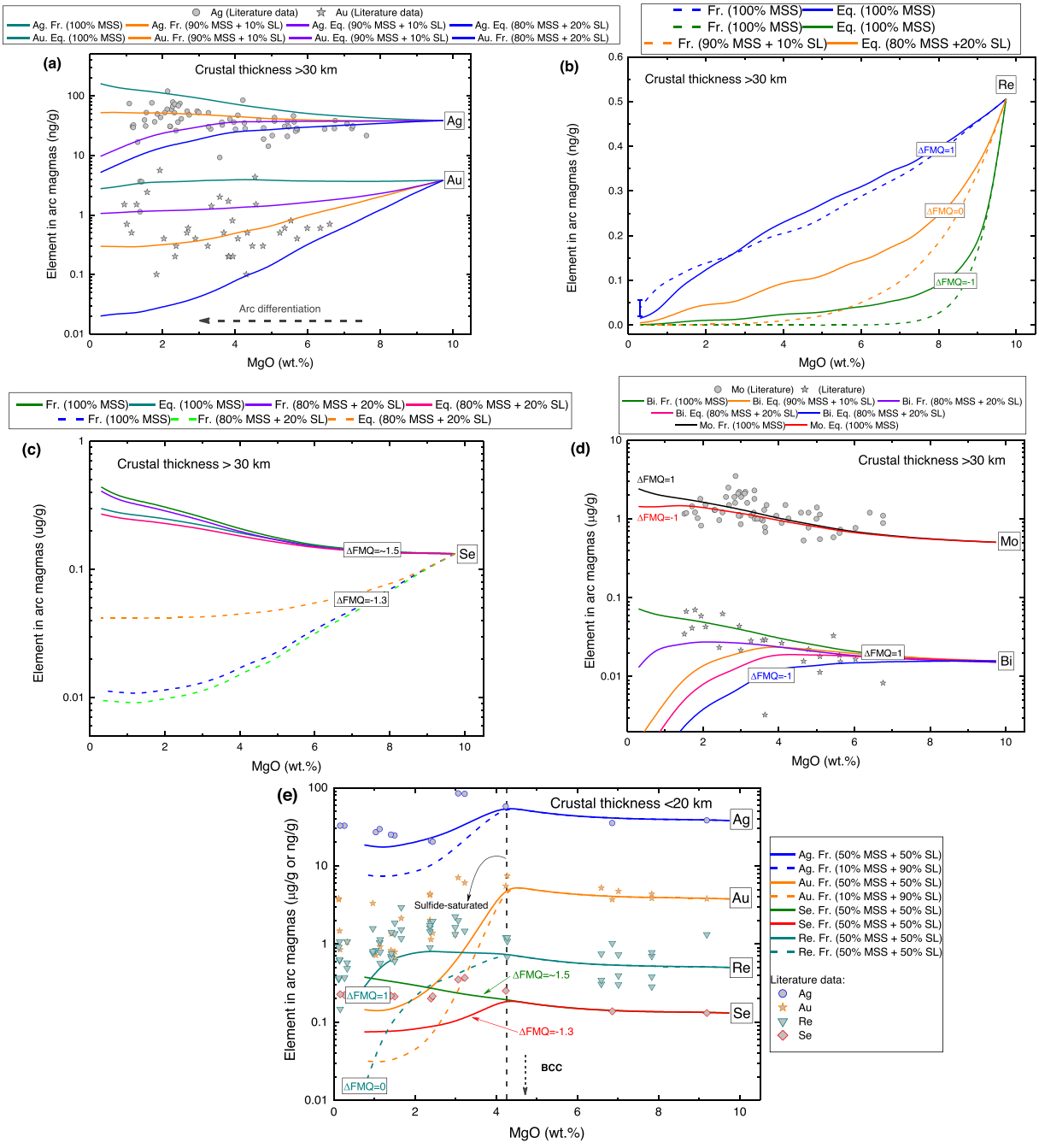

Fig. 8. Modeled evolution trends of the chalcophile elements Ag, Au, Re, Mo, Bi, and Se in arc magmas using the same fractional (Fr.) and equilibrium (Eq.) crystallization models as those used in Fig. 7 to model the evolution of Cu. Note that for Re, Mo, Bi, and Se also the effect of reduced conditions (ΔFMQ = −1.3 to 0) vs. oxidized conditions (ΔFMQ = 0–1.5) was considered, because the $D^{MSS/SM}$ and $D^{SL/SM}$ for these elements vary as a function of fO_2. Note that Au decreases significantly with increasing the proportion of sulfide liquid (a). Re decreases with decreasing MgO (b). Bi and Se decrease with decreasing MgO under reduced conditions (c, d), but Mo is less affected by fO_2 (d). The Au, Ag, Mo, and Bi contents in magmas of continental arcs (Cox et al., 2019; Kunz et al., 2020; Bai et al., 2020), and the Au, Ag, Re, and Se contents in back-arc (eastern Manus basin) magmas (Sun et al., 2003; Jenner et al., 2010; Park et al., 2013), were plotted for comparison with the modeling results. Note that the Au, Ag, Re, and Se data of the back-arc samples are systematically shifted from the modeling results, because the sulfide saturation occurred in these back-arc magmas at ~3 wt.% MgO, rather than at ~4.3 wt.% MgO as modeled for global arcs with a crustal thickness of <20 km. Available literature data of Re and Se in arc magmas of continental arcs were not plotted due to their loss during magmatic degassing. Note that the errors of the calculated element contents in arc magmas, caused by the standard deviation of the fitting (Table 4), are up to 50% relative for Re, as shown in (b), but are <10–15% for the other elements (not shown).

magmatic rocks for Au, Ag, Se, Mo, Re, and Bi. Overall, the natural sample data are consistent with the predicted results at fO_2 of FMQ to FMQ + 1. However, note that the data obtained for back-arc (eastern Manus basin) samples are systematically shifted from the predicted results, because the sulfide saturation occurred in these back-arc magmas at ~3 wt.% MgO, rather than at ~4.3 wt.% MgO as modeled for global arcs with a crustal thickness of <20 km. The large consistence between the predicted results and the observations for different chalcophile elements (Figs. 7 and 8) justifies the validity of our model setup and the reliability of our estimated mass and proportions of different sulfide phases precipitated during arc magmatic differentiation.

The predicted Cu, Au, Ag, Re, Se, Se, Mo, Pb, Bi, As, Sn, and Sb contents in arc magmas are also compared with their counterparts in Earth's bulk continental crust (BCC) withs similar MgO content of ~4.7 wt.% (Rudnick and Gao, 2014), as illustrated in Fig. 9. Fig. 9a shows that the predicted element contents in oxidized magmas (ΔFMQ = 1–1.5) at arcs with a crustal thickness of >30 km match well with those in the BCC, if the saturating

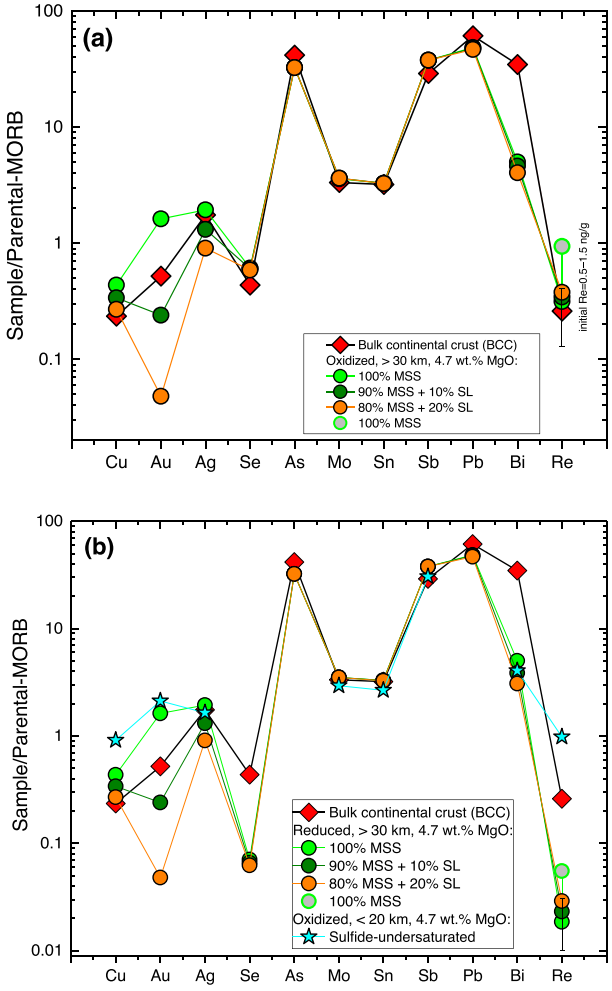

Fig. 9. Parental-MORB normalized chalcophile element abundance in arc magmas at ~4.7 wt.% MgO. Note that the abundances of all plotted chalcophile elements in arc magmas were calculated using the same approach as used in Figs. 7 and 8, but only the data obtained from the fractional crystallization model were plotted. Using the results from the equilibrium crystallization model would not change the general pattern. (a) The chalcophile element abundance in oxidized arcs (ΔFMQ = 1–1.5) with a crustal thickness >30 km matches well with the composition of the bulk continental crust if the precipitating sulfides are dominantly MSS in a proportion between 90% and 100%. (b) The Cu, Au, and Re abundance in reduced arcs (ΔFMQ ≤ 0) with a crustal thickness of >30 km, or in arcs with a crustal thickness of <20 km, does not match with the composition of the bulk continental crust. Under reduced conditions (ΔFMQ ≤ 0), Se and Re are too depleted in continental arcs to match with their abundance in the bulk continental crust. Due to sulfide undersaturation, Cu, Au, and Re are too enriched in island arcs to match with their abundance in the bulk continental crust. Note that 0.5–1.5 ng/g Re was considered in the parental arc basalt when modeling the behavior of Re during magmatic differentiation in continental arcs, but only 0.5 ng/g Re was used when modeling the behavior of Re during magmatic differentiation in arcs with a crustal thickness of <20 km. Also note that the errors for the plotted data of Cu, Ag, As, Mo, Sn, Sb, Pb, and Bi, caused by the standard deviation of the fitting (Table 4), are <10–15% relative, but are up to 50% for Re. The parental-MORB data used for normalization were taken from Jenner (2017).

sulfides are MSS in a proportion between 90% and 100%. The presence of sulfide liquid in a proportion more than 10% would deplete the magma in Au, compared to that in the BCC, whereas the presence of sulfides as 100% MSS would enrich the magma in Au. Fig. 9b further shows that Se and Re are significantly depleted in arc magmas if the fO_2 is below FMQ. Fig. 9b also shows that the Cu, Au, and Re contents in oxidized magmas at arcs with a crustal thickness of <20 km are much higher than their counterparts in the BCC because of sulfide-undersaturation in magmas at >~4.3 wt.% MgO.

The above results demonstrate that the main component of the BCC must have been formed in continental arcs and under oxidized conditions (ΔFMQ = 0–1), rather than in thin island arcs or under reduced conditions (ΔFMQ < 0). This conclusion is consistent with the constraints placed by Nb and Ta, that deep-seated magmatic differentiation in continental arcs is necessary to produce the low Nb/Ta signature of Earth's continental crust (Tang et al., 2019). The above results also demonstrate that during the formation of Earth's continental crust, magmatic Cu, Au, and Re are sequestered mainly by MSS and a small fraction of sulfide liquid in the deep continental crust, probably in deep crustal hot zones (Annen et al., 2006). Therefore, delamination of such sulfide-bearing mafic rocks from deep crustal hot zones into the convecting mantle can explain the observed Cu–Au–Re depletion in the BCC (Lee et al., 2012; Li and Audétat, 2013; Jenner, 2017; Feng and Li, 2019; Chen et al., 2020). However, under oxidized conditions this MSS + sulfide liquid assemblage sequesters only very limited amounts of the other chalcophile elements including Ag, Pb, Bi, Se, Mo, As, Sn, and Sb, which, together with the contributions of the subducting slab (Jenner, 2017), can explain the enrichments of these elements in the BCC.

5. CONCLUSIONS

We performed experiments at 1000–1200 °C, 0.5–1.0 GPa, and fO_2 1–1.5 log units above FMQ to determine the partition coefficients of Mn, Co, Cu, Zn, As, Se, Mo, Ag, Cd, Sn, Sb, Te, Re, Au, Pb, and Bi between MSS, Cu-rich sulfide liquid, and hydrous silicate melt of basaltic to dacitic compositions. The $D^{SL/SM}$ of Au increase with increasing Cu content of the sulfide liquid, but the $D^{SL/SM}$ of the other elements are not considerably affected by the Cu concentration in the sulfide liquid. We parameterized the $D^{SL/SM}$ and $D^{MSS/SM}$ of Mn, Co, Ni, Cu, Zn, As, Mo, Ag, Cd, Sn, Sb, Re, Pb, and Bi as a multi- function of temperature, pressure, fO_2, and compositions of the silicate melt and sulfide. This partitioning model can be used to predict $D^{SL/SM}$ and $D^{MSS/SM}$ for chalcophile elements in magmas under the shallow upper mantle to crust conditions. Our sulfide phase relations suggest that the sulfides precipitating from silicate melts containing >100 μg/g Cu occur as Cu-rich sulfide liquid, whereas the sulfides precipitating from silicate melts containing 30–70 μg/g Cu occur as mixed MSS and Cu-rich sulfide liquid. Our partitioning model was used to understand the behavior of chalcophile elements during arc magmatic differentiation. Modeling the Cu, Ag, As, Sn, Sb, Se, Mo, Re, Mo, Au, Pb, and Bi evolution trends of global arc magmas illustrates that the precipitating sulfides are dominantly MSS in continental arcs with a crustal thickness of >30 km, with the proportion of sulfide liquid being less than 20%; whereas, in island arcs with a crustal thickness of <20 km, the proportion of sulfide liquid may reach up to 90%. We find that when no more than 10% of the precipitating sulfides are sulfide liquid, the chalcophile element patterns of oxidized magmas (ΔFMQ = 0–1) in continental arcs well match with that of Earth's bulk continental crust, implying that Earth's continental crust formed mainly in oxidized continental arcs.

Declaration of Competing Interest

The authors declare that they have no known competing financial interests or personal relationships that could have appeared to influence the work reported in this paper.

ACKNOWLEDGEMENTS

This work is supported by National Key R&D Program of China (2018YFA0702600) and the National Natural Science Foundation of China (42021002) to Y.L. We would like to thank two anonymous reviewers for their constructive comments, and Zoltan Zajacz for his constructive comments and editorial handling of the manuscript.

APPENDIX A. SUPPLEMENTARY MATERIAL

Supplementary data to this article can be found online at https://doi.org/10.1016/j.gca.2021.03.020.

REFERENCES:

Agangi A. and Reddy S. M. (2016) Open-system behaviour of magmatic fluid phase and transport of copper in arc magmas at Krakatau and Batur volcanoes, Indonesia. *J. Volcanol. Geoth. Res.* **327**, 669–686.

Annen C., Blundy J. D. and Sparks R. S. J. (2006) The genesis of intermediate and silicic magmas in deep crustal hot zones. *J. Petrol.* **47**, 505–539.

Audetat A. and Pettke T. (2006) Evolution of a porphyry-Cu mineralized magma system at Santa Rita, New Mexico (USA). *J. Petrol.* **47**, 2021–2046.

Bai Z.-J., Zhong H., Hu R.-Z. and Zhu W.-G. (2020) Early sulfide saturation in arc volcanic rocks of southeast China: Implications for the formation of co-magmatic porphyry–epithermal Cu–Au deposits. *Geochim. Cosmochim. Acta* **280**, 66–84.

Beermann O., Botcharnikov R. E., Holtz F., Diedrich O. and Nowak M. (2011) Temperature dependence of sulfide and sulfate solubility in olivine-saturated basaltic magmas. *Geochim. Cosmochim. Acta* **75**, 7612–7631.

Bell A. S., Simon A. and Guillong M. (2009) Experimental constraints on Pt, Pd and Au partitioning and fractionation in silicate melt–sulfide–oxide–aqueous fluid systems at 800° C, 150MPa and variable sulfur fugacity. *Geochim. Cosmochim. Acta* **73**, 5778–5792.

Bockrath C., Ballhaus C. and Holzheid A. (2004) Fractionation of the platinum-group elements during mantle melting. *Science* **305**, 1951–1953.

Botcharnikov R. E., Holtz F., Mungall J. E., Beermann O., Linnen R. L. and Garbe-Schonberg D. (2013) Behavior of gold in a magma at sulfide-sulfate transition: Revisited. *Am. Mineral.* **98**, 1459–1464.

Botcharnikov R. E., Linnen R. L., Wilke M., Holtz F., Jugo P. J. and Berndt J. (2011) High gold concentrations in sulphide-bearing magma under oxidizing conditions. *Nat. Geosci.* **4**, 112–115.

Brenan J. M. (2002) Re–Os fractionation in magmatic sulfide melt by monosulfide solid solution. *Earth Planet. Sci. Lett.* **199**, 257–268.

Brenan J. M. (2008) Re–Os fractionation by sulfide melt–silicate melt partitioning: A new spin. *Chem. Geol.* **248**, 140–165.

Brenan J. M. (2015) Se–Te fractionation by sulfide–silicate melt partitioning: Implications for the composition of mantle-derived magmas and their melting residues. *Earth Planet. Sci. Lett.* **422**, 45–57.

Carroll M. and Rutherford M. J. (1988) Sulfur speciation in hydrous experimental glasses of varying oxidation state–results from measured wavelength shifts of sulfur X-rays. *Am. Mineral.* **73**, 845–849.

Chang J. and Audétat A. (2018) Petrogenesis and metal content of hornblende-rich xenoliths from two laramide-age magma systems in Southwestern USA: insights into the metal budget of arc magmas. *J. Petrol.* **59**, 1869–1898.

Chen K., Tang M., Lee C.-T. A., Wang Z., Zou Z., Hu Z. and Liu Y. (2020) Sulfide-bearing cumulates in deep continental arcs: The missing copper reservoir. *Earth Planet. Sci. Lett.* **531**.

Chiaradia M. (2014) Copper enrichment in arc magmas controlled by overriding plate thickness. *Nat. Geosci.* **7**, 43–46.

Cox D., Watt S. F. L., Jenner F. E., Hastie A. R. and Hammond S. J. (2019) Chalcophile element processing beneath a continental arc stratovolcano. *Earth Planet. Sci. Lett.* **522**, 1–11.

Feng L. and Li Y. (2019) Comparative partitioning of Re and Mo between sulfide phases and silicate melt and implications for the behavior of Re during magmatic processes. *Earth Planet. Sci. Lett.* **517**, 14–25.

Fraley K. J. and Frank M. R. (2014) Gold solubilities in bornite, intermediate solid solution, and pyrrhotite at 500° to 700° C and 100 MPa. *Econ. Geol.* **109**, 407–418.

Gaetani G. A. and Grove T. L. (1997) Partitioning of moderately siderophile elements among olivine, silicate melt, and sulfide melt: constraints on core formation in the Earth and Mars. *Geochim. Cosmochim. Acta* **61**, 1829–1846.

Georgatou A., Chiaradia M., Rezeau H. and Wälle M. (2018) Magmatic sulphides in Quaternary Ecuadorian arc magmas. *Lithos* **296–299**, 580–599.

Ghiorso, M.S., Hirschmann, M.M., Reiners, P.W., Kress III, V.C. (2002) The pMELTS: A revision of MELTS for improved calculation of phase relations and major element partitioning related to partial melting of the mantle to 3 GPa. 3, 1–35.

Hattori K. (1993) High-sulfur magma, a product of fluid discharge from underlying mafic magma: Evidence from Mount Pinatubo, Philippines. *Geology* **21**, 1083.

Hawkesworth C. J., Dhuime B., Pietranik A. B., Cawood P. A., Kemp A. I. S. and Storey C. D. (2010) The generation and evolution of the continental crust. *J. Geol. Soc. London* **167**, 229–248.

Jagoutz O. and Behn M. D. (2013) Foundering of lower island-arc crust as an explanation for the origin of the continental Moho. *Nature* **504**, 131–134.

Jagoutz O. and Kelemen P. B. (2015) Role of arc processes in the formation of continental crust. *Annu. Rev. Earth Planet. Sci.* **43**, 363–404.

Jégo S. and Dasgupta R. (2014) The fate of sulfur during fluid-present melting of subducting basaltic crust at variable oxygen fugacity. *J. Petrol.* **55**, 1019–1050.

Jenner F. E. (2017) Cumulate causes for the low contents of sulfide-loving elements in the continental crust. *Nat. Geosci.*.

Jenner F. E., Arculus R. J., Mavrogenes J. A., Dyriw N. J., Nebel O. and Hauri E. H. (2012) Chalcophile element systematics in volcanic glasses from the northwestern Lau Basin. *Geochem. Geophys. Geosyst.* **13**, n/a-n/a.

Jenner F. E., O'Neill H. S. C., Arculus R. J. and Mavrogenes J. A. (2010) The magnetite crisis in the evolution of arc-related magmas and the initial concentration of Au, Ag and Cu. *J. Petrol.* **51**, 2445–2464.

Jugo P. J. (2004) An experimental study of the sulfur content in basaltic melts saturated with immiscible sulfide or sulfate liquids at 1300 °C and 1.0 GPa. *J. Petrol.* **46**, 783–798.

Jugo P. J., Luth R. W. and Richards J. P. (2005) Experimental data on the speciation of sulfur as a function of oxygen fugacity in basaltic melts. *Geochim. Cosmochim. Acta* **69**, 497–503.

Jugo P. J., Wilke M. and Botcharnikov R. E. (2010) Sulfur K-edge XANES analysis of natural and synthetic basaltic glasses: Implications for S speciation and S content as function of oxygen fugacity. *Geochim. Cosmochim. Acta* **74**, 5926–5938.

Kelemen P. B. and Behn M. D. (2016) Formation of lower continental crust by relamination of buoyant arc lavas and plutons. *Nat. Geosci.* **9**, 197–205.

Kiseeva E. S. and Wood B. J. (2013) A simple model for chalcophile element partitioning between sulphide and silicate liquids with geochemical applications. *Earth Planet. Sci. Lett.* **383**, 68–81.

Kiseeva E. S. and Wood B. J. (2015) The effects of composition and temperature on chalcophile and lithophile element partitioning into magmatic sulphides. *Earth Planet. Sci. Lett.* **424**, 280–294.

Klimm K., Kohn S. C., O'Dell L. A., Botcharnikov R. E. and Smith M. E. (2012) The dissolution mechanism of sulphur in hydrous silicate melts. I: Assessment of analytical techniques in determining the sulphur speciation in iron-free to iron-poor glasses. *Chem. Geol.* **322–323**, 237–249.

Kullerud G. (1970) *Sulfide phase relations*. Mineralogical Society of America.

Kullerud G., Yund R. A. and Moh G. H. (1969) Phase Relations in the Cu-Fe-S, Cu-Ni-S, and Fe-Ni-S Systems*. In *Magmatic Ore Deposits* (ed. H. D. B. Wilson). Society of Economic Geologists.

Kunz B. E., Hammond S. J., Hastie A. R., Jenner F. E., Watt S. F. L. and Cox D. (2020) Elevated magma fluxes deliver high-Cu magmas to the upper crust. *Geology*.

Lanzirotti A., Lee L., Head E., Sutton S. R., Newville M., McCanta M., Lerner A. H. and Wallace P. J. (2019) Direct measurements of copper speciation in basaltic glasses: understanding the relative roles of sulfur and oxygen in copper complexation in melts. *Geochim. Cosmochim. Acta* **267**, 164–178.

Lee C. T., Luffi P., Chin E. J., Bouchet R., Dasgupta R., Morton D. M., Le Roux V., Yin Q. Z. and Jin D. (2012) Copper systematics in arc magmas and implications for crust-mantle differentiation. *Science* **336**, 64–68.

Lee, C.T.A. (2014) Physics and chemistry of deep continental crust recycling. 423–456.

Leitzke F. P., Fonseca R. O. C., Sprung P., Mallmann G., Lagos M., Michely L. T. and Münker C. (2017) Redox dependent behaviour of molybdenum during magmatic processes in the terrestrial and lunar mantle: Implications for the Mo/W of the bulk silicate Moon. *Earth Planet. Sci. Lett.* **474**, 503–515.

Li Y. (2014a) Chalcophile element partitioning between sulfide phases and hydrous mantle melt: Applications to mantle melting and the formation of ore deposits. *J. Asian Earth Sci.* **94**, 77–93.

Li Y. (2014b) Comparative geochemistry of rhenium in oxidized arc magmas and MORB and rhenium partitioning during magmatic differentiation. *Chem. Geol.* **386**, 101–114.

Li Y. (2018) Temperature and pressure effects on the partitioning of V and Sc between clinopyroxene and silicate melt: Implications for mantle oxygen fugacity. *Am. Mineral.* **103**, 819–823.

Li Y. and Audétat A. (2012) Partitioning of V, Mn Co, Ni, Cu, Zn, As, Mo, Ag, Sn, Sb, W, Au, Pb, and Bi between sulfide phases and hydrous basanite melt at upper mantle conditions. *Earth Planet. Sci. Lett.* **355**, 327–340.

Li Y. and Audétat A. (2013) Gold solubility and partitioning between sulfide liquid, monosulfide solid solution and hydrous mantle melts: Implications for the formation of Au-rich magmas and crust–mantle differentiation. *Geochim. Cosmochim. Acta* **118**, 247–262.

Li Y. and Audétat A. (2015) Effects of temperature, silicate melt composition, and oxygen fugacity on the partitioning of V, Mn Co, Ni, Cu, Zn, As, Mo, Ag, Sn, Sb, W, Au, Pb, and Bi between sulfide phases and silicate melt. *Geochim. Cosmochim. Acta* **162**, 25–45.

Li Y., Feng L., Kiseeva E. S., Gao Z., Guo H., Du Z., Wang F. and Shi L. (2019) An essential role for sulfur in sulfide-silicate melt partitioning of gold and magmatic gold transport at subduction settings. *Earth Planet. Sci. Lett.* **528**.

Liu Y. and Brenan J. (2015) Partitioning of platinum-group elements (PGE) and chalcogens (Se, Te, As, Sb, Bi) between monosulfide-solid solution (MSS), intermediate solid solution (ISS) and sulfide liquid at controlled fO2–fS2 conditions. *Geochim. Cosmochim. Acta* **159**, 139–161.

Mallmann G. and O'Neill H. S. C. (2007) The effect of oxygen fugacity on the partitioning of Re between crystals and silicate melt during mantle melting. *Geochim. Cosmochim. Acta* **71**, 2837–2857.

Masotta M. and Keppler H. (2015) Anhydrite solubility in differentiated arc magmas. *Geochim. Cosmochim. Acta* **158**, 79–102.

Masotta M., Keppler H. and Chaudhari A. (2016) Fluid-melt partitioning of sulfur in differentiated arc magmas and the sulfur yield of explosive volcanic eruptions. *Geochim. Cosmochim. Acta* **176**, 26–43.

Mengason M., Candela P. and Piccoli P. (2011) Molybdenum, tungsten and manganese partitioning in the system pyrrhotite–Fe–S–O melt–rhyolite melt: impact of sulfide segregation on arc magma evolution. *Geochim. Cosmochim. Acta* **75**, 7018–7030.

Metrich N. and Clocchiatti R. (1996) Sulfur abundance and its speciation in oxidized alkaline melts. *Geochim. Cosmochim. Acta* **60**, 4151–4160.

Mungall J. E. and Brenan J. M. (2014) Partitioning of platinum-group elements and Au between sulfide liquid and basalt and the origins of mantle-crust fractionation of the chalcophile elements. *Geochim. Cosmochim. Acta* **125**, 265–289.

Parat F., Holtz F. and Streck M. J. (2011) Sulfur-bearing magmatic accessory minerals. *Rev. Mineral. Geochem.* **73**, 285–314.

Park J.-W., Campbell I. H. and Arculus R. J. (2013) Platinum-alloy and sulfur saturation in an arc-related basalt to rhyolite suite: Evidence from the Pual Ridge lavas, the Eastern Manus Basin. *Geochim. Cosmochim. Acta* **101**, 76–95.

Peach C. and Mathez E. (1993) Sulfide melt-silicate melt distribution coefficients for nickel and iron and implications for the distribution of other chalcophile elements. *Geochim. Cosmochim. Acta* **57**, 3013–3021.

Rajamani V. and Naldrett A. (1978) Partitioning of Fe Co, Ni, and Cu between sulfide liquid and basaltic melts and the composition of Ni-Cu sulfide deposits. *Econ. Geol.* **73**, 82–93.

Ripley E. M., Brophy J. G. and Li C. (2002) Copper solubility in a basaltic melt and sulfide liquid/silicate melt partition coefficients of Cu and Fe. *Geochim. Cosmochim. Acta* **66**, 2791–2800.

Rowe M. C., Kent A. J. R. and Nielsen R. L. (2007) Determination of sulfur speciation and oxidation state of olivine hosted melt inclusions. *Chem. Geol.* **236**, 303–322.

Rowe M. C., Kent A. J. R. and Nielsen R. L. (2009) Subduction influence on oxygen fugacity and trace and volatile elements in basalts across the cascade volcanic arc. *J. Petrol.* **50**, 61–91.

Rudnick R. L. (1995) Making continental crust. *Nature* **378**, 571–577.

Rudnick R. L. and Gao S. (2014) Composition of the continental crust. *Treatise Geochem.* **4**, 1–51.

Simon A. C., Candela P. A., Piccoli P. M., Mengason M. and Englander L. (2008) The effect of crystal-melt partitioning on the budgets of Cu, Au, and Ag. *Am. Mineral.* **93**, 1437–1448.

Smythe D. J., Wood B. J. and Kiseeva E. S. (2017) The S content of silicate melts at sulfide saturation: New experiments and a model incorporating the effects of sulfide composition. *Am. Mineral.* **102**, 795–803.

Sun W., Bennett V. C., Eggins S. M., Kamenetsky V. S. and Arculus R. J. (2003) Enhanced mantle-to-crust rhenium transfer in undegassed arc magmas. *Nature* **422**, 294–297.

Tang M., Lee C. A., Chen K., Erdman M., Costin G. and Jiang H. (2019) Nb/Ta systematics in arc magma differentiation and the role of arclogites in continent formation. *Nat. Commun.* **10**, 235.

Taylor S. R. and McLennan S. (2009) *Planetary crusts: their composition, origin and evolution*. Cambridge University Press.

Wallace P. J. and Carmichael I. S. E. (1994) S speciation in submarine basaltic glasses as determined by measurements of SKa X-ray wavelength shifts. *Amer. Mineral.* **79**, 161–167.

Wallace P. J. and Edmonds M. (2011) The sulfur budget in magmas: evidence from melt inclusions, submarine glasses, and volcanic gas emissions. *Rev. Mineral. Geochem.* **73**, 215–246.

Wang Z., Becker H., Liu Y., Hoffmann E., Chen C., Zou Z. and Li Y. (2018) Constant Cu/Ag in upper mantle and oceanic crust: Implications for the role of cumulates during the formation of continental crust. *Earth Planet. Sci. Lett.* **493**, 25–35.

Wilke M., Klimm K. and Kohn S. C. (2011) Spectroscopic studies on sulfur speciation in synthetic and natural glasses. *Rev. Mineral. Geochem.* **73**, 41–78.

Williams H. M., Prytulak J., Woodhead J. D., Kelley K. A., Brounce M. and Plank T. (2018) Interplay of crystal fractionation, sulfide saturation and oxygen fugacity on the iron isotope composition of arc lavas: An example from the Marianas. *Geochim. Cosmochim. Acta* **226**, 224–243.

Zajacz Z., Candela P. A., Piccoli P. M., Sanchez-Valle C. and Wälle M. (2013) Solubility and partitioning behavior of Au, Cu, Ag and reduced S in magmas. *Geochim. Cosmochim. Acta* **112**, 288–304.

Zajacz Z., Candela P. A., Piccoli P. M., Wälle M. and Sanchez-Valle C. (2012) Gold and copper in volatile saturated mafic to intermediate magmas: Solubilities, partitioning, and implications for ore deposit formation. *Geochim. Cosmochim. Acta* **91**, 140–159.

Zhang Z. and Hirschmann M. M. (2016) Experimental constraints on mantle sulfide melting up to 8 GPa. *Am. Mineral.* **101**, 181–192.

Associate editor: Zoltan Zajacz